Gain-guiding effects in stimulated Raman scattering

by Philip Ross Battle

A thesis submitted in partial fulfillment of the requirements for the degree of Doctor of Philosophy in Physics
Montana State University

Abstract:
Measurements of the output of a Raman amplifier when there is no input Stokes seed are presented. It is shown that a fully quantum mechanical scaled planewave theory describes the growth from spontaneous emission well in the high gain limit. However, in the low gain regime there is a significant increase in the amount of Stokes output which is not predicted by the plane wave theory. To account for the deviation from planewave growth observed at low gain, a fully quantum mechanical theory of amplification in a focused gain geometry is presented. The theory is based on a non-orthogonal mode expansion of the amplified field and incorporates the effects of both gain-guiding and diffraction. In addition to accounting for the observed Stokes output at low gain the non-orthogonal mode theory predicts that the Stokes field cart experience enhanced gain as well as have excess noise. Results from an experiment are presented which verify the existence of enhanced gain in a multipass Raman amplifier. Though the experiment does not give a direct measure of the excess noise factor the results indicate that there may be more than the usual quantum limit of 1 photon of noise effectively seeding the Raman amplifier.

GAIN-GUIDING EFFECTS IN STIMULATED RAMAN SCATTERING

by

Philip Ross Battle

A thesis submitted in partial fulfillment
of the requirements for the degree

of

Doctor of Philosophy

in

Physics

MONTANA STATE UNIVERSITY
Bozeman, Montana

April 1993

APPROVAL

of a thesis submitted by

Philip Ross Battle

This thesis has been read by each member of the thesis committee and has been found to be satisfactory regarding content, English usage, format, citations, bibliographical style, and consistency, and is ready for submission to the College of Graduate Studies.

4-2-93
Date

John L Cayman
Chairperson, Graduate Committee

Approved for the Major Department

4-2-93
Date

Head, Major Department

Approved for the College of Graduate Studies

4/6/93
Date

Graduate Dean

STATEMENT OF PERMISSION TO USE

In presenting this thesis in partial fulfillment of the requirements for a doctoral degree at Montana State University, I agree that the Library shall make it available to borrowers under rules of the Library. I further agree that copying of this thesis is allowable only for scholarly purposes, consistent with "fair use" as prescribed in the U.S. Copyright Law. Requests for extensive copying or reproduction of this thesis should be referred to University Microfilms International, 300 North Zeeb Road, Ann Arbor, Michigan 48106, to whom I have granted "the exclusive right to reproduce and distribute my dissertation for sale in and from microfilm or electronic format, along with the right to reproduce and distribute my abstract in any format in whole or in part."

Signature____________________

Date 4/6/93

ACKNOWLEDGEMENTS

I would like to thank my advisor, John Carlsten, for allowing me the opportunity to work in his lab. His constant encouragement, inexhaustible patience, and boundless enthusiasm has made my tenure here a wonderful experience. Also I would like to thank Rand Swanson for introducing me to many of the interesting and fun ideas which this thesis is based on.

Thanks are also due to the students in John's lab. I am indebted to Jim Wessel for the many hours of insightful and sometimes whimsical conversation and the seemingly endless hours spent working with me on experiments. In addition I would like to acknowledge the many useful discussions with Tim Heumier and Meg Hall.

I am also grateful for the expert advise given by Erik Anderson and Norm Williams.

Further, I wish to thank Dr. Robiscoe and Dr. Cone for their critical reading of this thesis. Their comments and suggested revisions have been incorporated into this thesis.

Perhaps the people I owe the most are my friends outside the physics department. In particular I wish to thank Marilou Turrentine, David Wilson, and Tim Fry for the countless hours of fun we have had together.

Finally I owe my family more than I'll ever be able to repay. Throughout my academic career they have been a constant source of support and encouragement.

TABLE OF CONTENTS

LIST OF FIGURES

LIST OF FIGURES - Continued

ABSTRACT

Measurements of the output of a Raman amplifier when there is no input Stokes seed are presented. It is shown that a fully quantum mechanical scaled planewave theory describes the growth from spontaneous emission well in the high gain limit. However, in the low gain regime there is a significant increase in the amount of Stokes output which is not predicted by the plane wave theory. To account for the deviation from planewave growth observed at low gain, a fully quantum mechanical theory of amplification in a focused gain geometry is presented. The theory is based on a non-orthogonal mode expansion of the amplified field and incorporates the effects of both gain-guiding and diffraction. In addition to accounting for the observed Stokes output at low gain the non-orthogonal mode theory predicts that the Stokes field can experience enhanced gain as well as have excess noise. Results from an experiment are presented which verify the existence of enhanced gain in a multipass Raman amplifier. Though the experiment does not give a direct measure of the excess noise factor the results indicate that there may be more than the usual quantum limit of 1 photon of noise effectively seeding the Raman amplifier.

CHAPTER 1

INTRODUCTION

The term Raman scattering is used to describe an inelastic photon scattering process. When a photon scatters off a Raman active medium it can either deposit or extract energy from the medium depending on the initial state of the medium. Though Raman scattering is typically done using the vibrational and/or rotational states of molecules in a gas or liquid it can also be done using electronic states of an atom or can occur through an interaction of the incident photon with lattice or phonon modes of a solid.

When a photon is red shifted in the Raman process it is commonly referred to as a Stokes photon. In Fig.1 an energy level diagram of the Stokes process is shown. The Raman active molecule starts in the ground state $|1\rangle$. An incident pump photon with energy $\hbar\omega_p$ scatters off the molecule leaving it in level $|3\rangle$. In order to conserve energy the scattered Stokes photon energy is given by $\hbar\omega_s = \hbar\omega_p - \hbar\omega_{31}$. The Raman process can also lead to blue shifted photons referred to as anti-Stokes photons.

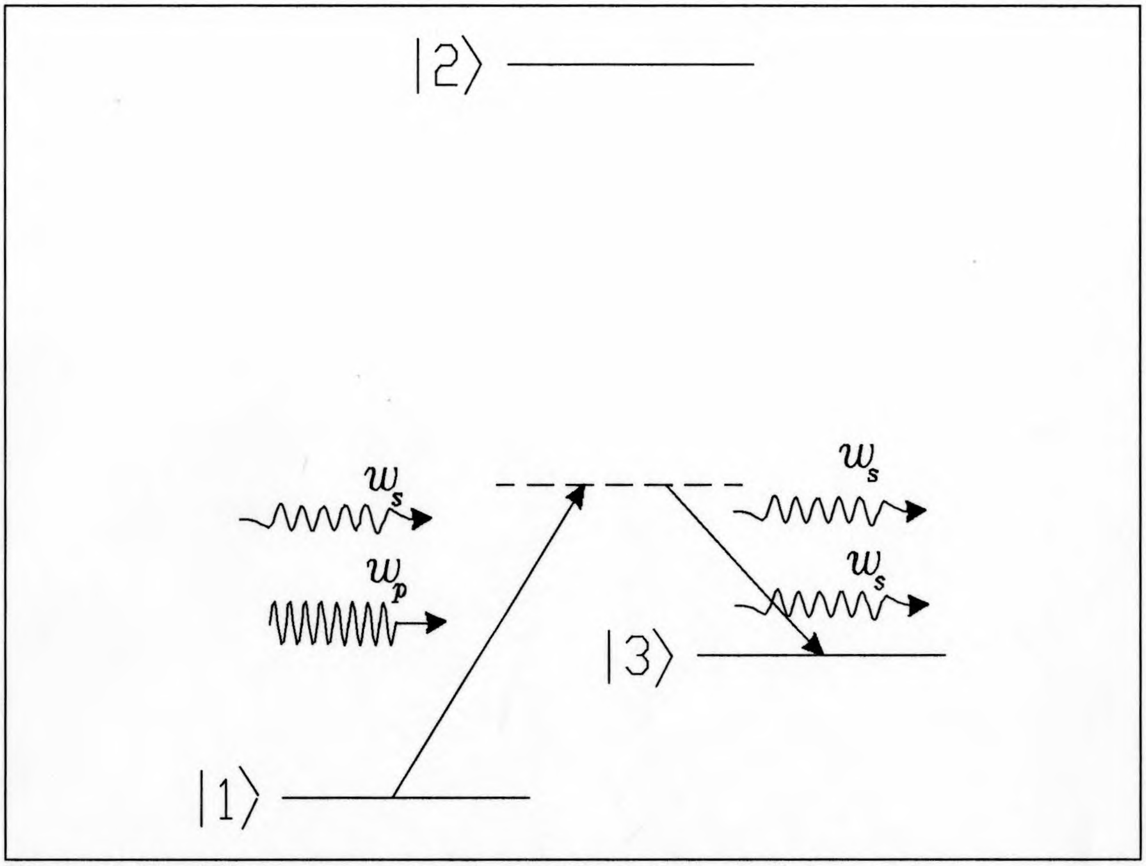

Figure 1 Simplified energy level diagram for Raman scattering process

There are two scattering mechanisms which contribute to the production of anti-Stokes photons. The non-resonant contribution to anti-Stokes scattering occurs when the pump photon scatters off a molecule which starts in the excited state, $|3\rangle$. The scattered photon is blue shifted in energy and the molecule is left in the ground state, $|1\rangle$. In resonant or coherent anti-Stokes scattering (CARS) the blue shifted photon results from a four-wave mixing between the Stokes and pump fields. In this case the molecule starts in the ground state and ends there as well. For both paths energy conservation dictates

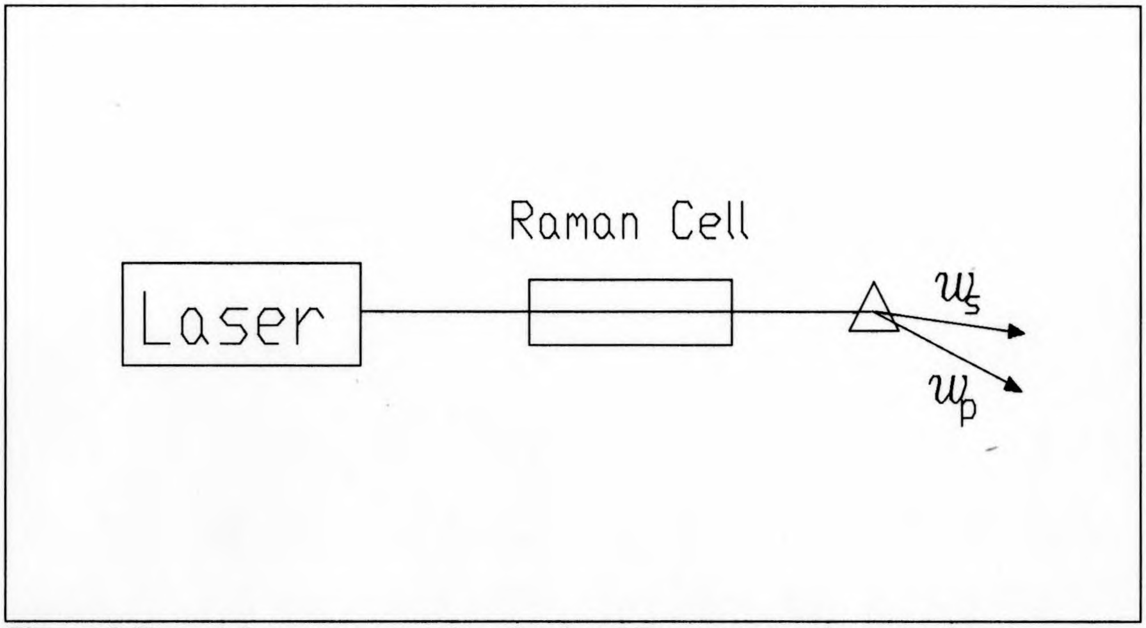

Figure 2 Essential components of a stimulated Raman scattering experiment.

that the resulting anti-Stokes photon has an energy given by $\hbar\omega_{AS}=\hbar\omega_p+\hbar\omega_{31}$.

Stokes scattering can occur spontaneously or, as alluded to in Fig.1, can be stimulated by other Stokes photons which are incident on the molecule at the same time the pump photon interacts with the molecule. The latter process is referred to as stimulated Raman scattering. Even in the absence of an initial Stokes field, stimulated Raman scattering can still occur. In Fig.2 the essential details of a Raman scattering experiment are shown. An intense laser is used to pump a Raman active medium. Since no Stokes photons are incident with the pump field only spontaneous Raman scattering occurs. However some of the initial spontaneous Stokes photons travel in the direction of the pump and are subsequently amplified through the stimulated Raman process discussed above. Exploring both experimentally and theoretically the various aspects of quantum initiated stimulated Raman scattering is the central theme of this thesis.

Background and Motivation

Stimulated Raman scattering(SRS), although actively studied since 1962,[1] continues to be an important and exciting research field as well as a practical and useful tool. Along with the well known applications in spectroscopy[2-5] such as generation of efficient tunable lasers in the infrared, SRS has recently been used to generate very narrow linewidth pulses.[6] In the non-linear regime it has been shown that the equations describing SRS admit soliton solutions.[7] These solitons have been observed to occur spontaneously and recently much effort has gone into studying and understanding the role of quantum fluctuations in the generation and propagation of the SRS solitons.[8-11]

SRS has also been used to gain insight into the microscopic quantum world, through amplification of the vacuum field the microscopic quantum fluctuations are manifest in frequency, time, spatial and energy fluctuations of the macroscopic output Stokes field.[12-15] In addition it has been demonstrated both theoretically and experimentally that a Raman amplifier can be operated at the phase insensitive quantum noise limit of 1 photon per mode.[16,17] In this thesis I present and discuss experimental data on SRS generation in a multipass cell (MPC).

There are several advantages to doing SRS, as well as other stimulated emission processes, in a MPC. In a MPC, the amplified field and the pump field are focused on each pass. In a focused geometry where the confocal parameter of the pump field is small compared to the medium length the threshold for amplification is minimized.[6,18,19]

The MPC can also be used to increase the gain. The gain enhancement is due to the multiple passes which effectively increase the length of the medium. This gain enhancement, which can easily be as much as an order of magnitude with the use of a MPC,[24] is extremely useful in cases where the gain is very small, such as SRS of CO_2 lasers in the IR.

As well as threshold reduction and gain enhancement, the MPC provides an excellent arena for studying first Stokes generation and amplification since focusing and wavelength selective mirrors each reduce the gain of higher order emission processes. For example, it has been shown that for single focus SRS, the ratio of anti-Stokes to Stokes is reduced to the 10^{-3} level.[18,20] For a MPC configured with mirrors that reflect strongly only at the Stokes and pump wavelengths the anti-Stokes to Stokes ratio is further reduced, and other four-wave mixing processes such as second or higher order Stokes are inhibited. In addition, the MPC can be configured, as in our experiment, so that the transit time of the pump through the MPC is greater than the temporal width of the pump. In this configuration the growth of backward Stokes is also greatly reduced. Thus the amplification of the Stokes pulse in a MPC can be studied without the usual complications of higher order mixing processes which accompany a high gain single pass system.

In both the experimental and theoretical work discussed in this thesis the Raman medium used was molecular hydrogen. Molecular hydrogen, H_2, is a homonuclear diatomic molecule. In Fig.3 a detailed (though not to scale) diagram of the energy levels

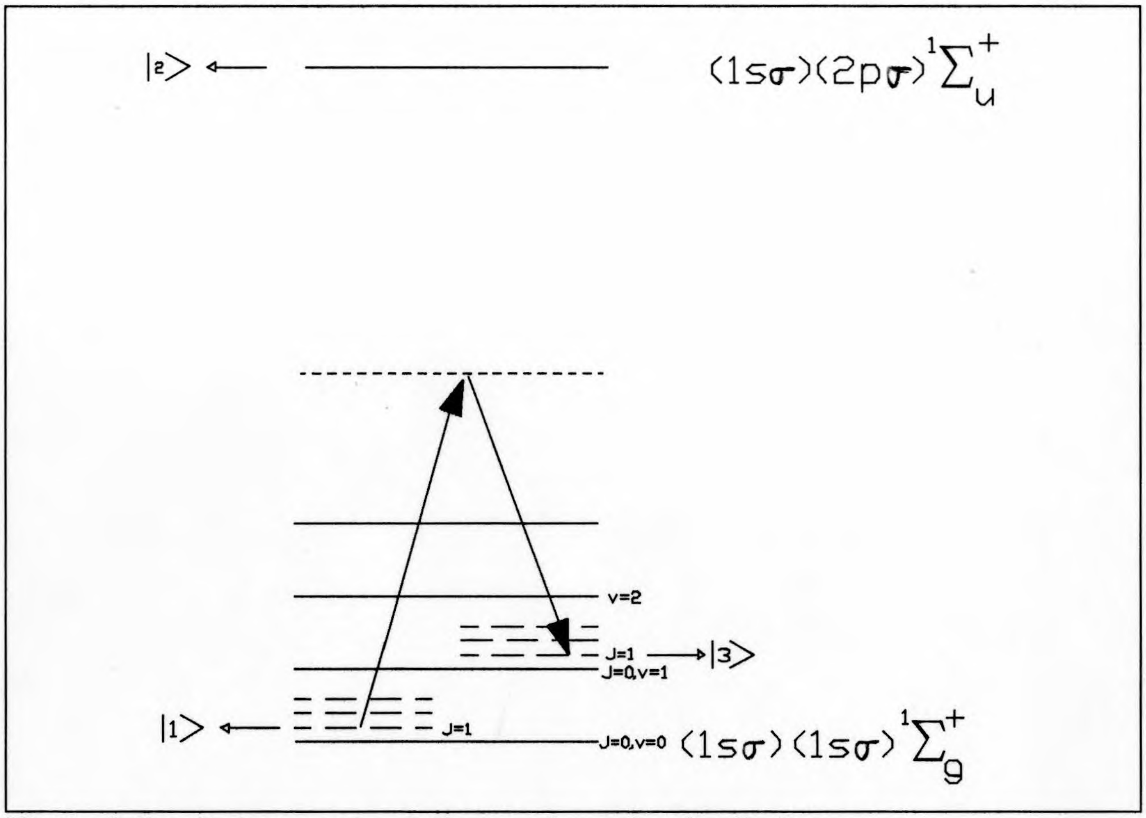

Figure 3 Detailed energy level diagram for molecular Hydrogen.

for H_2 is shown. The ground electronic state is denoted $(1s\sigma)(1s\sigma)\ ^1\Sigma_g^+$, where Σ indicates that the state has zero projected angular momentum, the indices + and g indicate the symmetry properties of the electronic wavefunction and the superscript 1 indicates that the electrons are in a singlet spin configuration.[21] The coarsely-spaced energy levels above the ground state are due to the vibrational degree of freedom in the molecule and are denoted by v=0,1,2.. . The first few vibrational levels are separated in energy by approximately 0.5 eV. In addition, for each vibrational level there is a finer energy level structure corresponding to the rotational degrees of freedom which are denoted by J=0,1,2... and are separated in energy by approximately 0.03eV. The first electronic excited state denoted $(1s\sigma)(2p\sigma)\,{}^1\Sigma_u^+$, is separated from the ground state by approximately 90,000cm^{-1} or 11.2eV. Though not shown, there is a similar coarse and fine scale energy level structure associated with this state.

Raman scattering transitions amongst these levels do not take place arbitrarily but are constrained by the selection rules $\Delta v=0, \Delta J=0,\pm2$ or $\Delta v=\pm1, \Delta J=0,\pm2$. Because in our work the pump photons were linearly polarized, we only had to consider pure vibrational Raman scattering, $\Delta v=\pm1, \Delta J=0$. The nomenclature used to label pure vibrational transitions is $Q_{v,v'}(J)$ where v is the initial vibrational level, v' is the final vibrational level and J is the rotational state of the molecule.

At room temperature, which is the temperature at which our work was done, the molecule is primarily in the ground electronic state with v=0. However, due to the combined nuclear and rotational degeneracies, a majority of the molecules(66%) populate the J=1 rotational state rather then the lowest, J=0, rotational state. The following correspondences can be made to the simplified energy level diagram given in Fig.1; the ground state, $|1\rangle$, corresponds to the electronic ground state $(1s\sigma)^2\,{}^1\Sigma_g^+$

with v=0 and J=1, level $|2\rangle$ is identified as the first electronic excited state, and level $|3\rangle$ again corresponds to the ground electronic state but now has v=1 and J=1. This is summarized by saying that Raman scattering was done using the $Q_{01}(1)$ branch of H_2. In this case a pump photon at 532nm(green) undergoing Raman scattering will be Stokes shifted to become a photon at 683nm(red).

In the following chapter a brief description of the fully quantum mechanical plane wave theory of stimulated Raman scattering is presented. The theory accounts for both quantum initiation and propagation of the Stokes field. In addition we present a method for extending the jurisdiction of this theory to Raman scattering in a multipass cell. Finally we show the results of several experiments which point out some limitations of the plane wave theory in describing the growth from spontaneous emission in a multipass cell.

In Chapter 3 we develop a general three dimensional theory of steady state amplification in a focused gain geometry. The theory is based on a nonorthogonal mode expansion of the amplified field. The implications of including both the effects of diffraction and focused gain are explored. We show that the gain-guided nature of a focused-gain amplifier can have a large and profound effect on its output. In particular our analysis shows that the gain of the field can become larger than the usual plane wave gain and that the amount of noise effectively seeding the amplified field can be larger than the usual quantum limit of one photon per mode.

In Chapter 4 we summarize the results of two experiments designed to look for the excess noise in output of the gain-guided Raman amplifier. The experiments were performed using essentially the same apparatus as in the first set of experiments described in Chapter 2. The only notable change was the replacement of our old Nd:YAG laser with a new injection seeded YAG laser that might rightly be characterized as the "cadillac" of YAG's. The results of the experiments indicate that gain-guiding can indeed affect the noise properties of SRS.

Finally Chapter 5 concludes with a brief summary of the results in each of these chapters. In addition, directions that future work could follow are discussed.

CHAPTER 2

GROWTH FROM SPONTANEOUS EMISSION IN STIMULATED RAMAN SCATTERING

Recently, in one of the many theoretical and experimental investigations of amplification in a multipass cell (MPC),[20,22-24] Mac Pherson *et al.* demonstrated that, for stimulated Raman scattering (SRS) in the visible, amplification of an input Stokes pulse is well described by a semi-classical transient plane wave theory, even in the non-linear regime where pump depletion is significant. The focusing and multiple passes that occur in the MPC were accounted for by simply scaling the plane wave gain coefficient. In this chapter we show that the growth from spontaneous emission can also be described by a fully quantum mechanical transient plane wave theory, but only for relatively high gain. In the high gain regime we find that if the gain coefficient is scaled in the same manner as previous work[4;20,24] the growth of the Stokes field is well described.

In the low gain regime we find there is much more Stokes energy observed than predicted by the simple scaled plane wave theory. In order to obtain an insight into the origin of the excess Stokes energy, we considered the full three dimensional propagation/amplification problem. The solution to this was presented by Perry *et al.*,[22] for the case of steady state growth. By including the effects of spontaneous emission phenomenologically we are able to calculate the Stokes intensity from the MPC. In the low gain regime, we find that the effects of higher order spatial modes become significant, indicating that a simple transient plane wave model is no longer adequate to describe the Stokes growth.

Plane Wave Theory of Stimulated Raman Scattering

Raman scattering is driven by a coherent interaction between the medium, a pump field and a Stokes field. The beating of the pump and Stokes field produce a coherence between states $|1\rangle$ and $|3\rangle$ in the Raman active medium which, for our experiment, correspond to the ground state and first vibrational state in H_2. The induced molecular coherence then couples back to the pump field to produce the non-linear polarization at the Stokes frequency, $P_{nl}^{\omega_s} \sim (E_p^* E_s) E_p = |E_p|^2 E_s$. Stimulated Raman scattering (SRS) occurs because the rate of Stokes growth, which is proportional to the nonlinear polarization, is directly proportional to the amount of Stokes present. This implies that the Stokes growth will have exponential character, a hallmark of stimulated emission processes.

On first inspection of the non-linear polarization given above, one might conclude that if there is no injected Stokes field in the medium then, because the polarization is "zero", no Raman scattering occurs. Experimentally, however, this is not the case; when a Raman active medium is pumped in the absence of an initial Stokes field, spontaneous Raman scattering is observed. This apparent paradox is resolved when a fully quantum mechanical description of Raman scattering is considered.

In the fully quantum mechanical approach both the molecular response and the Stokes field are quantized. Then, just as the harmonic oscillator in its ground state has zero point fluctuations, the Stokes field, even with no photons in it, also has quantum zero point fluctuations. It is these quantum fluctuations in the Stokes field, often referred to as vacuum fluctuations, which are the origin of spontaneous Stokes scattering. A compelling feature of the fully quantum mechanical approach is that it ties together two seemingly distinct scattering mechanisms; using this model spontaneous emission can be thought of as simply, stimulated emission of the vacuum field.

A fully quantum mechanical description of plane wave amplification process for SRS has been presented by Raymer and Mostowski.[25] In deriving the Maxwell-Bloch equations that account for both growth and propagation of the Stokes field, they consider a collection of molecules in a pencil shaped region of length l_m and cross sectional area, A, uniformly pumped by a plane monochromatic field. The assumptions made are that the medium is left primarily in the ground state, and the pump field remains undepleted. In the absence of pump depletion, the output Stokes field $\hat{E}_s(z,\tau)$ is related linearly to the input Stokes field $\hat{E}_s(0,\tau)$, where $\tau = t - z/c$ is the retarded time, and z labels the position of some point along the axis of the amplifier. $\hat{E}_s^{(-)}(z,\tau)$

is the slowly varying negative frequency amplitude of the Stokes electric field

$$\hat{E}_s(z,\tau)=\hat{E}_s^{(+)}(z,\tau)e^{-i\omega_s\tau} + \hat{E}_s^{(-)}(z,\tau)e^{i\omega_s\tau} \; . \tag{2.1}$$

In terms of the retarded time parameter, the differential equations describing the growth of the Stokes field and its coupling to the medium are given by

$$\frac{\partial}{\partial z}\hat{E}_s^{(-)}(z,\tau)=-ik_2\hat{Q}^\dagger(z,\tau)E_p(z,\tau) \tag{2.2a}$$

and

$$\frac{\partial}{\partial \tau}\hat{Q}^\dagger(z,\tau)=-\Gamma\hat{Q}^\dagger(z,\tau)+ik_1E_p^*(z,\tau)\hat{E}_s^{(-)}(z,\tau)+\hat{F}^\dagger(z,\tau) \tag{2.2b}$$

where $\hat{Q}^\dagger(z,\tau)$ represents the polarization fluctuations in the medium, $\hat{F}^\dagger(z,\tau)$ is a quantum Langevin operator added to account for collisional dephasing, and Γ is the dephasing rate in the Raman medium. Also, in Eq.(2.2) k_1 and k_2 are constants related to the field-molecule coupling strength[25] and can be expressed in terms of the plane wave gain coefficient, α, by $k_1k_2=\dfrac{\Gamma c\alpha}{16\pi}$

Though somewhat disguised, the first equation, 2.2a, is simply the steady state slowly varying form of Maxwell's wave equation. The right hand side of this equation is proportional to the non-linear polarization which is produced from the coupling between the induced molecular coherence, $\hat{Q}^{\dagger}(z,\tau)$ and the pump field E_p. The second equation, 2.2b, represents growth of the molecular coherence which results from the beating of the pump and Stokes fields.

The solution to Eq.(2.2) in terms of the Stokes field $\hat{E}_s^{(-)}(z,\tau)$ can be found in ref.[25]. The average Stokes power is related to the expectation value of the normally ordered product of the Stokes field and can be written as[26]

$$P_s(\tau)=\frac{Ac}{2\pi}\langle\hat{E}_s^{(-)}(z,\tau)\hat{E}_s^{(+)}(z,\tau)\rangle \tag{2.3}$$

$$=gz\,|\gamma(\tau)|^2\Gamma\hbar\omega_s\left(\frac{1}{2}+gz\Gamma\int_0^{\tau}d\tau'\,|\gamma(\tau')|^2e^{-2\Gamma(\tau-\tau')}\frac{I_1^2(\sqrt{q(\tau,\tau')})}{q(\tau,\tau')}\right).$$

where the pump field has the form $E_p(\tau)=E_o\gamma(\tau)$, $g = \alpha I_p$ and I_1 is a modified Bessel function of first order. In the steady state, $\Gamma\tau_p \gg 1$, high gain limit the Stokes intensity increases exponentially with increasing pump power. In this limit Eq.(2.3) becomes

$$P_s\approx\frac{\hbar\omega_s\Gamma}{2(\pi gz)^{1/2}}e^{gz} \tag{2.4}$$

which resembles the usual semi-classical high gain result and justifies calling α the plane wave gain coefficient.

Extension to a Multipass Cell

A theoretical investigation of amplification in a focused gain geometry, such as a multipass cell, has shown that when the gain per pass is small the spatial modes which describe the growth act independently.[22] Additionally when the amplified field's wavelength is comparable to the pump field's wavelength only one mode has dominant growth.[22] For SRS with a visible laser, the above conditions can easily be met and thus single mode growth can be expected. Previous theoretical and experimental studies of Raman amplification in a MPC have shown that Stokes amplification can be described by a plane wave theory.[20,23] In this approach, however, the usual gain length coefficient, gz, is scaled to account for the focusing and multiple passes.

In the next section we compare the output from a Raman generator in a MPC to the fully quantum mechanical plane wave theory presented above. As in previous work, to account for focusing, we replace the non-uniformly pumped geometry by a uniformly pumped region with an effective area given by[20]

$$A_{eff}=\frac{l_m(\lambda_s+\lambda_p)}{4\tan^{-1}(l_m/b)} \tag{2.5}$$

where, as shown in Fig.4, l_m is the medium length and b is the confocal parameter of the system which depends on the MPC mirror spacing. The effective area is defined in this way so that the pump intensity,

$$I_p = \frac{P_p}{A_{eff}}$$

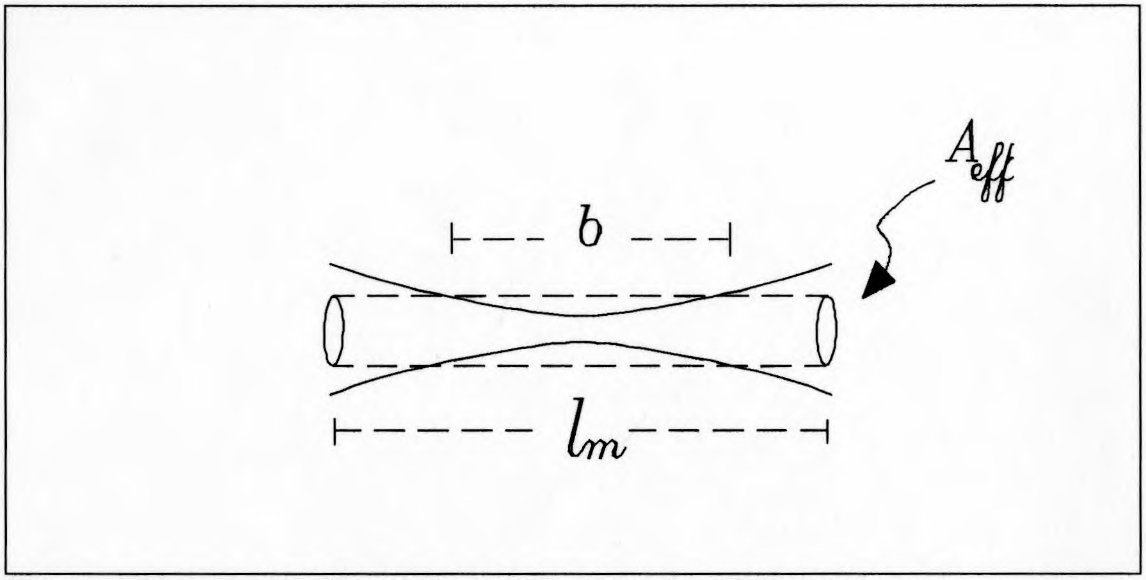

Figure 4 Diagram showing relationship between A_{eff} and focused pump geometry.

gives the same total gain over a length l_m as does a focused pump beam with the same power and a confocal parameter b.[23] To account for losses resulting from the multiple passes through the medium an effective length is used which is given by[20]

$$z_{eff} = l_m \frac{T(1-(T^2R)^s)}{(1-(T^2R))} \tag{2.6}$$

where T is the transmission of the Raman cell, R is the reflectivity of the MPC mirrors and s is the number of passes. Note that in the limit of zero losses (T=R=1) Eq.(2.6) goes to $z_{eff}= sl_m$ so that the effective length is just the length times the number of passes.

Combining the solution to the plane wave theory, Eq.(2.3), with the expression given for the effective area, Eq.(2.5), and the effective length, Eq.(2.6), allows one to calculate the growth, in a MPC, of the Stokes pulse from spontaneous emission.

Experimental Setup and Results

The experimental setup used to test the validity of this model is shown in Fig.5. The major elements in the system are a single mode Nd:YAG pump laser, a Raman generator, and three energy detectors. One detector monitors the pump and the other two detect the Stokes energy at different intensity levels.

The Raman generator consists of a cell of H_2 filled to a given pressure in the range of 3 atmospheres to 30 atmospheres. The Raman scattering, done at room temperature, occurs predominantly at the $Q_{01}(1)$ transition. As shown in Fig.5 the Raman cell is simply placed between the mirrors of the MPC. Further details of the experimental set up can be found in Appendix A.

In Fig. 6 we have plotted the logarithm of the Stokes output energy vs. input pump energy. The data shown were taken at 26.4 and 3.2 atmospheres. The transmission loss in the MPC as well as the loss from the cell to the detectors were measured and folded out of the data, allowing a direct comparison with the theory. Each

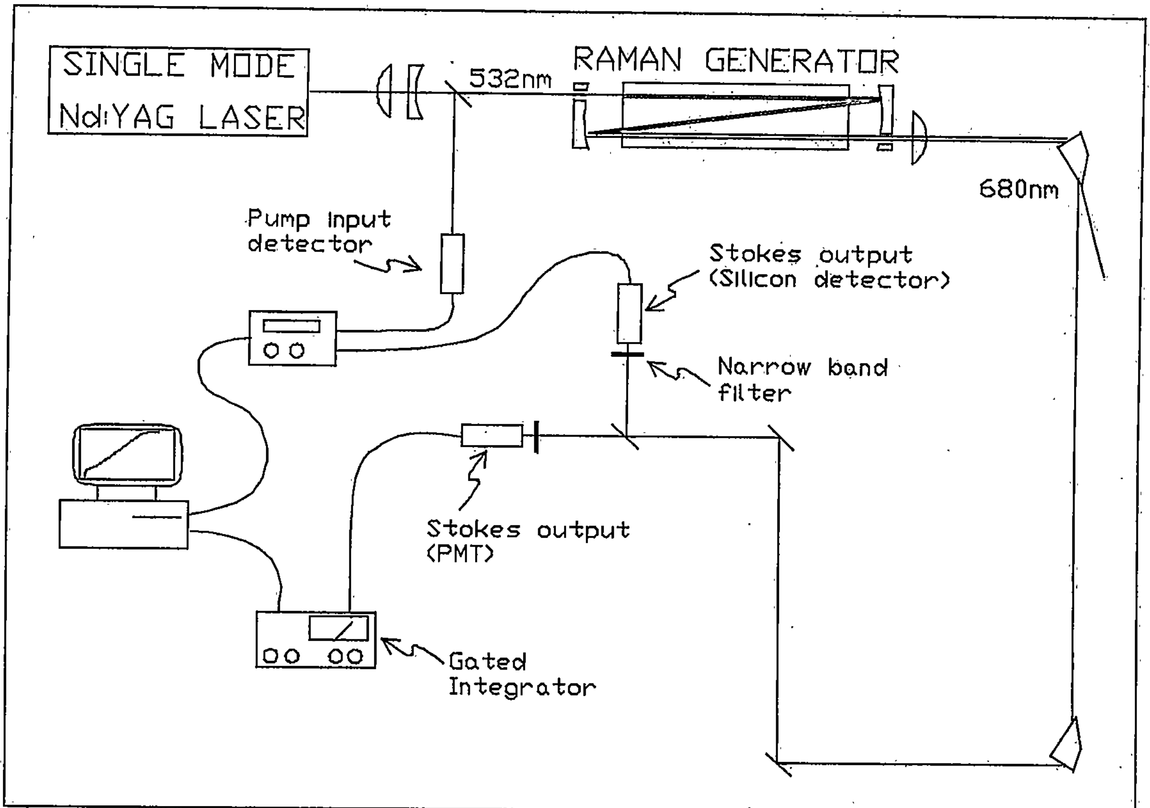

Figure 5 Experimental apparatus used to measure Stokes growth from spontaneous emission in a H_2 Raman multipass cell.

data point represents an ensemble average of at least 100 Stokes shots collected at a given pump energy (within ±3%). The error bars shown include both statistical and systematic error and are representative of the size of the errors on all the points. The statistical errors are inherent in both the quantum nature of Stokes build up and in the fluctuations in detection caused by finite quantum efficiency of the detectors. The systematic errors arise from uncertainty in energy meter calibration and error in the measurement of transmission and reflection coefficients of the optical elements. For Stokes energies less than 10^{-14}J the vertical error bars become quite large due to the uncertainty inherent in matching the output of the PMT to the absolute energy scale of

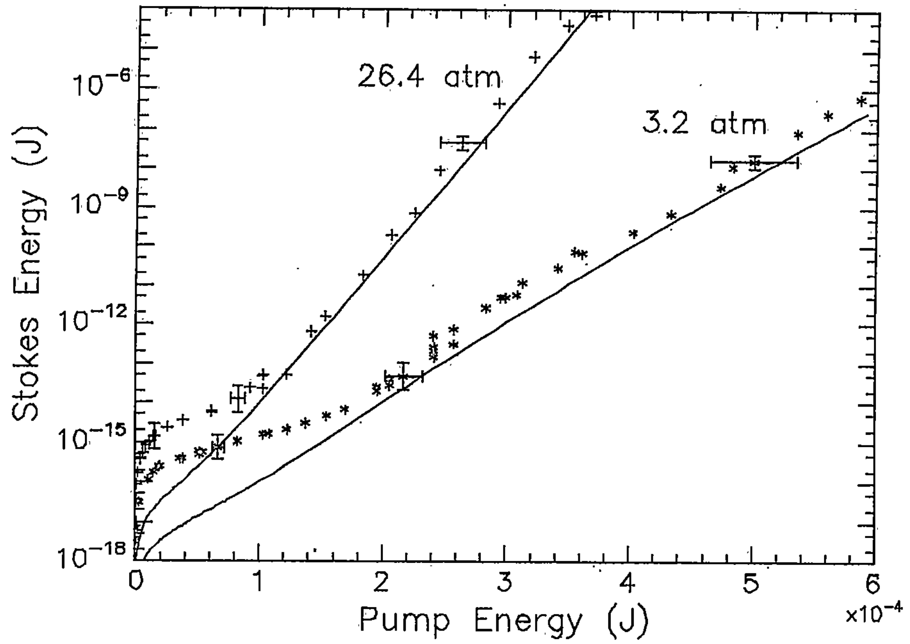

Figure 6 Stokes energy as a function of pump energy at two different pressures. Individual data points are experimental, while the solid lines represent the scaled transient plane wave theory.

the silicon detector.

The solid lines in Fig.6 represent the scaled transient plane wave theory discussed at the beginning of this chapter. The theoretical curve is produced by numerically integrating the Stokes power, Eq.(2.3), over the pump temporal profile, resulting in the ensemble averaged Stokes energy at a given pump energy. The theoretical curves in Fig.6 were calculated using no free parameters. As discussed earlier, the effect of focusing is accounted for by scaling the plane wave gain length product, as given in Eq.(2.5) and Eq.(2.6). The plane wave gain coefficient and the Raman linewidth are calculated using the work of Bischel and Dyer[28]; their values for these experiments can be found in Appendix A.

As is apparent from Fig.6 the predicted gain and the measured gain (slope) agree remarkably well for the two pressures shown; we found this to be the case for 10 atmospheres as well. There does, however, appear to be some discrepancy between the overall measured energy output and that predicted by the theory. At this point it is unclear if this offset is an experimental artifact or due to some subtlety which is not properly accounted for by this theory. Future experiments using an injected signal from a tunable diode laser should help answer this question.

Since the small gain portion of Fig.6 deviates from the theory by a large amount,

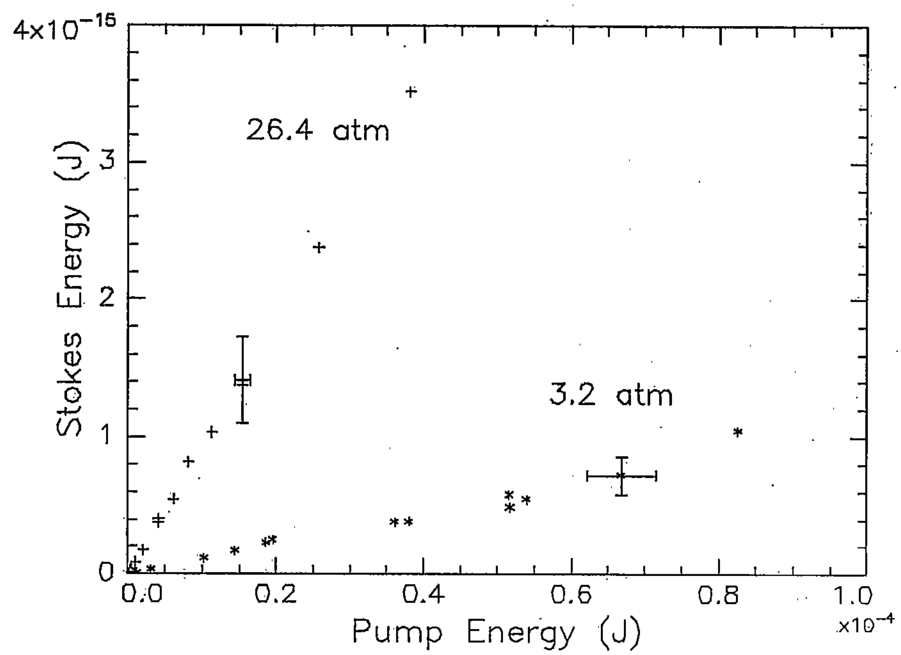

Figure 7 Stokes energy versus pump energy on a linear scale. These data show that the Stokes growth at low gains is linear and scales with pressure as expected.

it is useful to expand this portion of the curve; this is done in Fig. 7 for both the 26.4 and 3.2 atmosphere data. The data presented reflect only the output of the PMT. Also, the error bars shown do not include the uncertainty associated with calibrating the PMT output to the silicon detector output. Even though the theory does not accurately predict the small gain data obtained, it does predict that, in the low gain regime, the amount of spontaneous Stokes photons is directly proportional to the number of molecules, or pressure, in the cell. In Fig.7, it is seen that the output of the 26.4 atmosphere cell is approximately an order of magnitude higher than output of the 3.2 atmosphere cell, consistent with the theory. This leads us to conclude that this excess signal is not an experimental artifact, perhaps due to pump contamination of the signal or instrument error, but is indeed excess Stokes output.

For clarity we plot the 26.4 atmos. data again (Fig.8); however, the horizontal axis is now in terms of the parameter gz. Again, the transient plane wave, quantum theory is plotted as a solid line. It is evident from our results, that the fully quantum transient plane wave theory, when scaled to account for the multiple passes and focusing, describes the growth of Stokes pulse reasonably well for $gz \geq 10$. Though not shown we also found this to be the case for 3.2 and 10 atmospheres as well. However, as is apparent in Fig.8 there is a large discrepancy between the output predicted by the plane wave theory and the measured output for $gz \leq 10$.

To account for the excess signal at low gain we have considered the work of Perry *et al.*[22] They solve the propagation and amplification problem for a system with focused gain in steady state. By including spontaneous emission phenomenologically

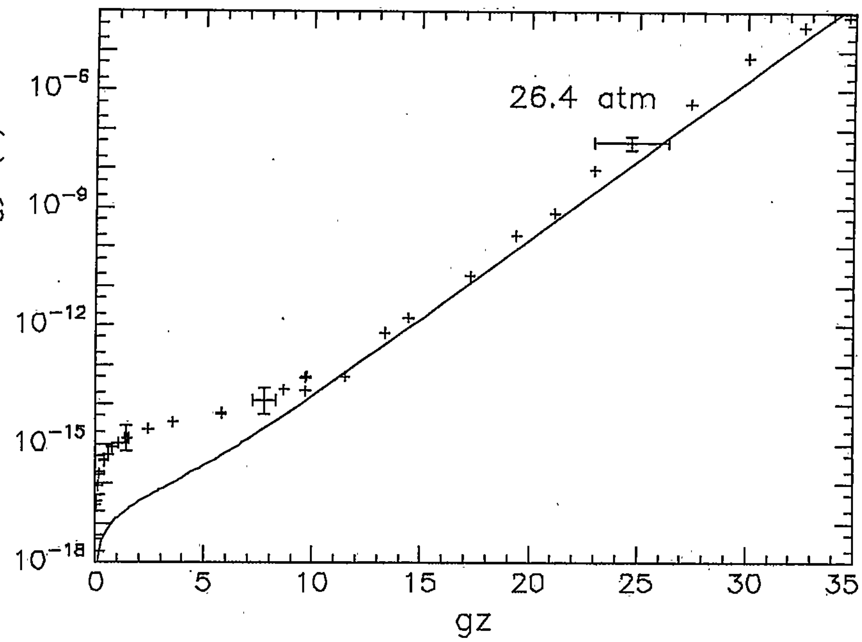

Figure 8 Stokes energy as a function of the gain-length parameter, gz. The solid line represents the scaled plane wave theory.

we generate the curve shown in Fig.9, which represents the growth of the Stokes field as a function of the gain length parameter gz. Also shown in Fig.9 (dashed curve) is the single mode steady state theory.[30] As is apparent from the figure, there is a large deviation from single mode growth for gz $\leq$ 10. The excess signal in this case is due to spontaneous emission into higher order spatial modes. If one looks carefully at the solid line in Fig.8, one can see a similar but smaller effect in the transient theory (solid line) at low gain. In this theory the deviation from a straight line at low gain is due to the phenomenon of temporal gain narrowing,[25] as the system gains fewer temporal modes become relevant. Thus, to adequately describe the Stokes growth in the low gain

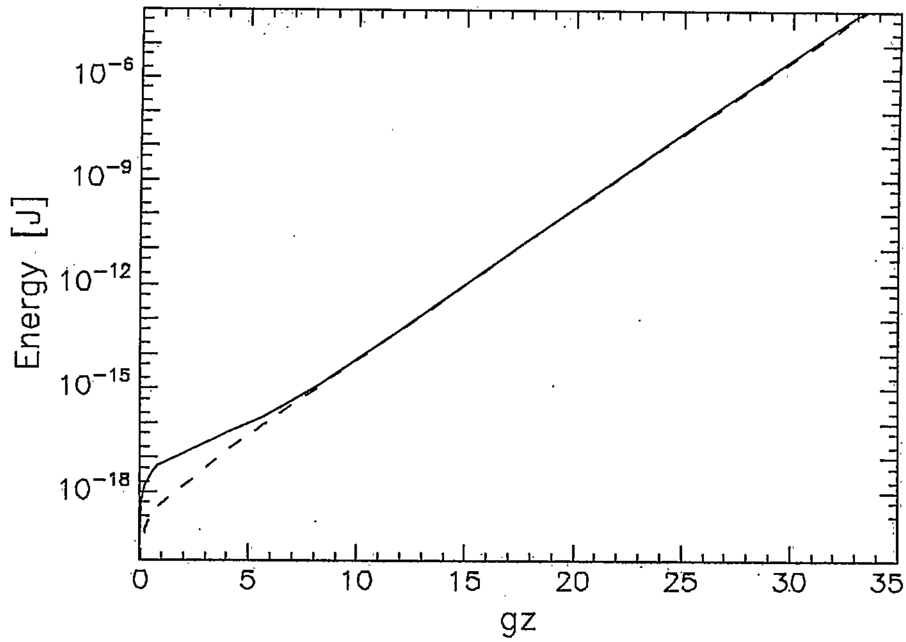

Figure 9 Comparison of the single mode steady state theory (dashed line) and the steady state focused gain theory(solid line). This indicates that higher order spatial modes contribute at low gain.

regime a theory needs to include both the effects of transiency and the effects of three dimensional propagation.

A fully quantum mechanical solution to the Stokes growth in a focused gain geometry will be presented in the next chapter. However we can get a qualitative picture of how the higher order modes contribute to the Stokes growth by combining the transient and focused gain theory in an approximate manner. Since, in the low gain steady state regime, the temporal modes act independently,[17] the two effects are simply multiplied; for each temporal mode several spatial modes must be included. The number of spatial modes, at a given gain, is estimated from the ratio of the focused gain result

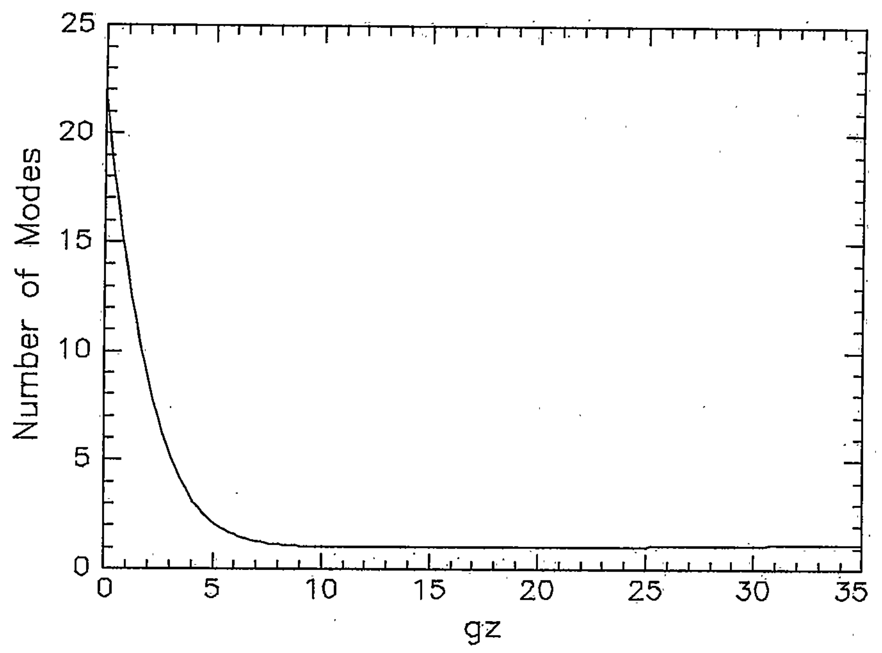

Figure 10 An estimate of the number of spatial modes which have significant gain vs. gz. At high gain only one mode is important. At lower gain more modes contribute.

of Perry *et al.* to the single mode theory. We plot this ratio as a function of gz in Fig.10. Note that in the low gain region, where there is not much gain discrimination, several spatial modes are populated due to spontaneous emission into these modes. However, as the gain increases only the lowest order spatial mode has dominant growth; it is in this region that the output of the amplifier is described well by the scaled transient plane wave theory.

If we approximate the gain for each spatial mode to be the same as the transient plane wave gain, given in Eq.(2.3), then the effect of additional spatial modes can be accounted for by scaling the transient theory by the number of additional spatial modes.

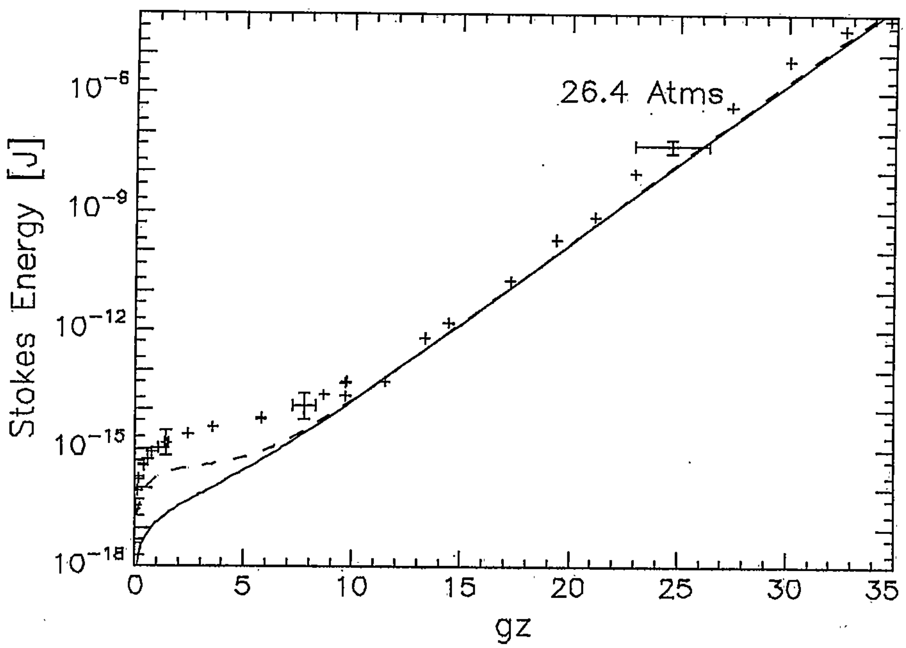

Figure 11 Comparison of experimental results to the combined focused gain and scaled plane wave theories (dashed curve). The scaled plane wave theory is also shown (solid line). The results indicate that higher order modes are important.

In Fig.11 the result of the modified transient theory(dashed line) is compared with the 26 atmosphere data; also shown is the unmodified transient theory(solid line). As is apparent from Fig.11, including the effects of the additional spatial modes dramatically increases the theoretical Stokes output for gz $\leq$ 10. The theory and experiment still don't agree in absolute Stokes output energy, but the overall shape of the respective curves is now in reasonable agreement over the whole gain regime. Thus it seems apparent that the experimentally observed excess noise, observed in the low gain regime, is the result of population in both higher order spatial modes and temporal modes.

In the next chapter we present a general theory for the quantum initiated output of an amplifier with focused gain. The non-Hermitian character of the gain-guided amplification process leads naturally to a description of the amplified field in terms of a non-orthogonal mode basis. In addition to accounting for the observed output in the low gain the theory indicates that the amplified field can be strongly affected by the gain-guided nature of the amplification process. In particular we show that the gain of the amplified field can be enhanced over the plane wave gain and that there can be more than the usual quantum limit of 1 photon per mode effectively seeding the mode. Both these effects are collectively referred to in the literature as excess noise.

CHAPTER 3

GAIN-GUIDING EFFECTS IN A FOCUSED GAIN AMPLIFIER

Optical systems in which the amount of noise effectively seeding the mode is larger than the usual quantum limit are said to have excess noise.[31-34] Examples of systems where excess noise may occur include laser resonators with high output coupling, unstable resonators, and gain-guided amplifiers. In the latter two systems the excess noise is associated with the transverse modes, while in the former case it is associated with the longitudinal modes of the system. What these systems all have in common is that they are described by wave equations which are non-Hermitian or have boundary conditions which are non-Hermitian.[33]

Petermann was first to show that the non-Hermitian nature of a gain-guided laser diode could lead to excess noise in the output field.[31] Though first mired in controversy, the existence of excess noise in optical systems is now well established. Excess noise has been predicted to play a role in a variety of phenomena including the build up of transverse coherence in X-ray lasers,[35] larger spectral linewidths in laser diodes,[36] and beam pointing fluctuations in gain-guided amplifiers.[37]

In the case of a gain-guided amplifier it is the presence of the gain term in the wave equation which makes the equation non-Hermitian. Past studies of excess noise properties of gain-guided amplifiers have considered gain profiles which are functions of the transverse coordinates only.[35,37] However, that approach is unrealistic for systems in which the gain region varies along the direction of propagation, as in the case of a focused gain profile.

In an amplifier with a non-uniform transverse gain profile the amplified field may experience transverse gain narrowing. This is due to the fact that the field near the peak of the gain profile grows more than at the sides, and thus naturally begins to narrow. For the case of a focused gaussian gain profile Perry *et al.* solved for the output intensity by expanding the amplified field into a set of orthogonal Gauss-Laguerre modes.[22] They found that, through amplification, the growth of these modes was coupled, which led to an enhancement of the field gain as well as transverse gain narrowing.

In this chapter we are interested in describing the growth from spontaneous emission in a focused gain amplifier. The output field is found by solving Maxwell's wave equation; to account for spontaneous emission a quantum Langevin operator, representing the polarization fluctuations in the medium, is included. In contrast to Perry's work, we begin by expanding the field into a set of non-orthogonal modes. By forcing the modes to satisfy a non-Hermitian equation we are led to a general expression for the growth of the amplified field from spontaneous emission. The expression predicts both gain enhancement and the amount of excess noise in the amplified field. Our analysis shows that as the non-orthogonal mode gain becomes larger than the usual scaled plane wave gain, the amount of noise effectively seeding the mode also increases. From this we conclude that a measurement of enhanced gain is also an indication that excess spontaneous emission (or excess noise) is present.

Quantum Theory of Focused Gain Amplification

The electric field operator for a field traveling in the positive z direction having a single transverse polarization can be expressed as a sum of its positive and negative frequency parts,

$$\hat{E}(t,z,\boldsymbol{r}_T)=\hat{E}^{(+)}(z,\boldsymbol{r}_T)e^{i(kz-\omega t)}+\hat{E}^{(-)}(z,\boldsymbol{r}_T)e^{-i(kz-\omega t)} \quad . \tag{3.1}$$

In Chapter Two the Stokes electric field was decomposed in a similar manner but because we were only considering plane wave growth the slowly varying amplitude did not depend on the transverse coordinate, $\mathbf{r}_T$. For this work we are interested in optical systems in which the growth of the amplified field can be described by the slowly varying Maxwell equation in the steady state paraxial limit. Then, in CGS units, the amplified field obeys[34,37]

$$\left(\nabla_T^2-2ik\partial_z+ik\,g(z,\boldsymbol{r}_T)\right)\hat{E}^{(-)}(z,\boldsymbol{r}_T)=-k^2 4\pi\hat{P}_{sp}^{\dagger}(z,\boldsymbol{r}_T) \tag{3.2}$$

where $\nabla_T^2=\partial_x^2+\partial_y^2$, $g(\mathbf{r}_T,z)$ represents the gain profile and $k=\omega/c$. To account for spontaneous emission we have included a quantum Langevin operator, $\hat{P}_{sp}(z,\boldsymbol{r}_T)$, which represents the quantum fluctuations in the polarization of the medium.

The formalism is purposely kept general in this work to stress the broad range of applicability. However it is not difficult to see the correspondence between Eq.(3.2) and the coupled set of equations describing stimulated Raman scattering presented in Chapter 2. First the transverse Laplacian must be included in Eq.(2.2a) so that the effect of diffraction is accounted for in Stokes propagation. Then if $\hat{Q}(z,\tau)$ is replaced in Eq.(2.2a) by its steady state value, found by setting $\frac{\partial \hat{Q}^{\dagger}}{\partial t}=0$ in Eq.(2.2b), we find that the resulting equation, which describes three dimensional steady state stimulated Raman scattering is identical to Eq.(3.2) when the following identifications are made; the operator used to account for the spontaneous emission, $\hat{P}^{\dagger}_{sp}$ is identified with $\hat{F}$ the quantum Langevin operator representing collisional dephasing in the Raman medium and the gain profile, $g(z,\boldsymbol{r}_T)$, is proportional to $|E_p(z,\boldsymbol{r}_T)|^2$.

The presence of the gain term (loss if g is negative) in Eq.(3.2) makes the wave equation non-Hermitian. If $g(z,r_T)$ were imaginary then the wave equation would be Hermitian and the optical system would be index-guided. In order to have amplification the gain term must have a non-zero real part which implies the equations describing amplification will always have some non-Hermitian character. For this work we consider a focused gaussian gain profile,

$$g(z,\mathbf{r}_T) = \frac{2g_o}{\pi w_g^2(z)} e^{\frac{-2r^2}{w_g^2(z)}} \tag{3.3}$$

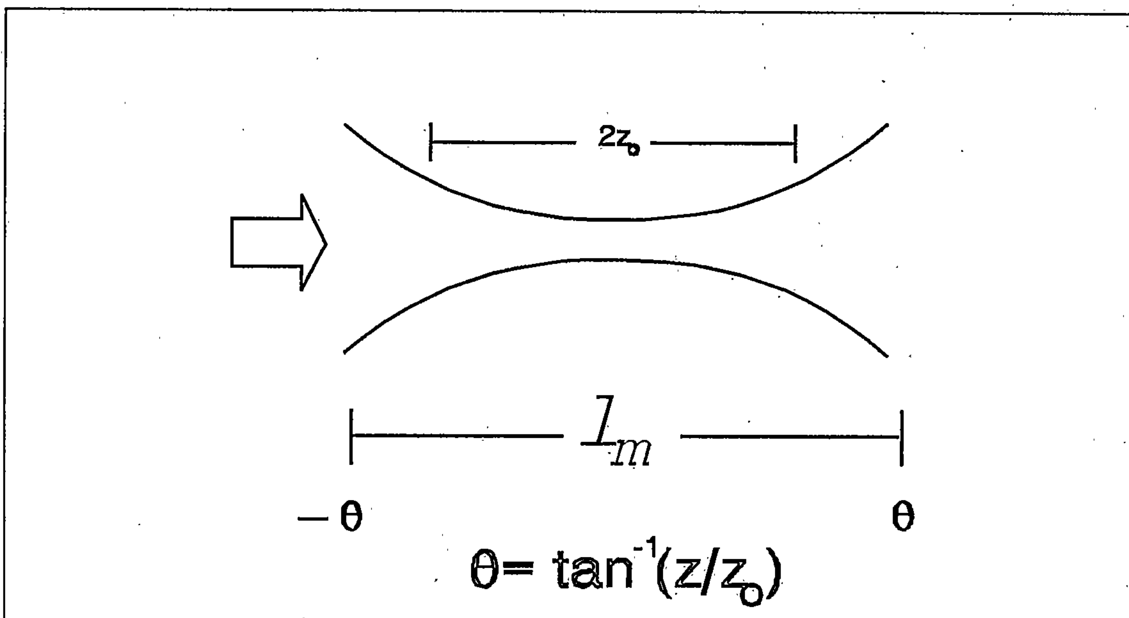

Figure 12 Schematic of the focused-gain geometry.

where $w_g^2(z)=w_g^2(0)(1+(z/z_o)^2)$, z_o is the Rayleigh range, r is the magnitude of the transverse position vector $\mathbf{r}_T$ and g_o is related to the peak gain coefficient. In Fig.12 a schematic of the focused gain geometry is shown. As we will see, the effect of defining the variable θ is to fold out the focused nature of the system.

To solve Eq.(3.2), the amplified field is expanded into a set of non-orthogonal modes,

$$\hat{E}^{(-)}(z,\boldsymbol{r}_T) = \sum_{n,l} \hat{a}_n^{l\dagger}(z)\Phi_n^l(z,\boldsymbol{r}_T) \tag{3.4}$$

where $\hat{a}_n^{l\dagger}$ is a generalized creation operator[34] for the photons in the non-orthogonal mode $\Phi_n^l(z,\boldsymbol{r}_T)$. We require the modes to satisfy the eigenvector equation

$$\left(\nabla_T^2 - 2ik\partial_z + ik\,g(z,\boldsymbol{r}_T)\right)\Phi_n^l(z,\boldsymbol{r}_T) = \lambda_n^l \frac{4ik}{k_g w_g^2(z)}\Phi_n^l(z,\boldsymbol{r}_T) \tag{3.5}$$

where λ_n^l is the eigenvalue associated with the mode $\Phi_n^l(z,\boldsymbol{r}_T)$ and k_g is defined by $k_g = \dfrac{2z_o}{w_g^2(0)}$. The indices n and l correspond to the radial and angular degrees of freedom respectively. In contrast to previous work[31,32,34,35,37] in which the gain function was not a function of z, the modes defined above are necessarily a function of z because of the focused nature of the gain profile. In the limit when the gain is zero the modes defined by Eq.(3.5) are related to the solution of the free space wave equations which in cylindrical coordinates are the Gauss-Laguerre functions.[22] As we will see the modes which solve this equation provide a natural basis in which to describe the amplified field.

Because the modes $\Phi_n^l(z,r_T)$ are solutions to a non-Hermitian equation they have some unusual but exciting properties. For instance, they are not orthogonal to each other in the standard power orthogonal sense. Another interesting aspect of these modes is the fact that they are not guaranteed to form a complete set. Completeness for these modes depends on the choice of gain profile and must be proved on a case by case basis.[39]

As mentioned above, it is generally true that the usual power orthogonality conditions for the modes do not hold. This is a consequence of the non-Hermitian nature of the equation that these modes satisfy. The standard power orthogonality relation is supplanted by

$$B_{n,m}^{l} = \int d^2 r_T \Phi_m^{l*} \Phi_n^l \tag{3.6}$$

which is a measure of the overlap between the non-orthogonal modes. An interesting point here is that even though the modes are functions of z, the overlap between modes does not change with z. Because the overlap between different modes is non-zero, noise can be transferred between modes and thus the noise in different modes is correlated.[32,33,35,37] The quantity $(B^{l}_{n;n})^2$ is referred to as the excess spontaneous emission or Petermann factor for the mode $\Phi^{l}_{n}(z,\boldsymbol{r}_T)$ and is greater than or equal to unity.[2,4]

There does exist a bi-orthogonality relationship, with another set of modes, $\psi^{l}_{n}(z,\boldsymbol{r}_T)$, referred to as the adjoint modes, which are related to solutions of the Hermitian adjoint of the differential operator in Eq.(3.5). Physically, the adjoint modes correspond to modes of a field traveling in the negative z direction.[33,34] The bi-orthogonality condition is written as

$$\int d^2 r_T \psi^{l*}_{m} \Phi^{l}_{n} = \delta_{m,n} \quad . \tag{3.7}$$

In Appendix B an explicit solution for the modes found from solving Eq.(3.5) is presented. In addition some properties of the bi-orthogonal modes, as well as the normalization choice, are also discussed.

With the modes of the amplifier determined, we turn our attention next to solving for the evolution of the operators in Eq.(3.4). In particular we want to solve for the correlation between the modes, $<\hat{a}^{l\dagger}_{n}\hat{a}^{l}_{m}>$. This expression can then be used to determine the total output power in the amplified field.

Substituting the field expansion, Eq.(3.4), into Eq.(3.2) leads to an equation of motion for the generalized creation operators,

$$\sum_n -2ik\Phi_n^l(\partial_z \hat{a}_n^{l\dagger} + \lambda_n^l \frac{2}{k_g w_g^2(z)} \hat{a}_n^{l\dagger}) = -k^2 4\pi \hat{P}_{sp}^{\dagger}(z,\boldsymbol{r}_T) \ . \tag{3.8}$$

If we assume that the spontaneous correlation function $\langle \hat{P}_{sp}^{\dagger}(z,\boldsymbol{r}_T)\hat{P}(z',\boldsymbol{r}_T')\rangle$ is delta correlated in space, which is the case for a generic two level amplifier[33,34] as well as for Raman scattering,[37] then an expression for the evolution of the operators can be determined; this is done in Appendix C.

The total output power in the amplified field is determined from

$$P = \frac{c}{2\pi}\int d^2r_T \langle \hat{E}^{(-)}(z,\boldsymbol{r}_T)\hat{E}^{(+)}(z,\boldsymbol{r}_T)\rangle = \frac{c}{2\pi}\sum_{n,j,m,l} \langle \hat{a}_n^{j\dagger}\hat{a}_m^{l}\rangle \int d^2r_T \Phi_m^{j*}\Phi_n^l \tag{3.9}$$

Note that, because the modes are non-orthogonal the total power is not just a sum of the power from each mode but has contributions from the cross terms as well. Substituting Eq.(3.6) and the expression for the correlation between the modes, found in Appendix C, into Eq.(3.9) leads to

$$P = \Delta\nu\hbar\omega \sum_l \sum_{n,m} (B_{n,m}^l)^2 \left(e^{(\lambda_n^l + \lambda_m^{l*})(\theta - \theta_o)} - 1\right) \tag{3.10}$$

where $\Delta\nu$ is the Hertzian bandwidth of the applied field and for simplicity, we have assumed a completely inverted system and that there is no injected signal.

The transformation from z to the new propagation variable θ has the effect of folding out the focused nature of the gain profile. Thus the growth of the amplified field is a simple exponential in θ. When the Rayleigh range, z_0, of the amplifying field is large compared to the medium length, the propagation parameter, θ, can be approximated as z/z_0. In this limit Eq.(3.10) reduces to a form similar to those found in theories which consider excess noise in systems where the gain profile is a function of transverse coordinates only,[35,37] i.e. longitudinally invariant. In addition, because of the positive definite character of the gaussian gain profile, Eq.(3.10) can be used to characterize the growth of the field over the whole gain region. This is in contrast to previous work which considered a parabolic gain profile where, because higher order modes experience negative gain, growth in the low gain regime could not be adequately described.[37]

The utility of the non-orthogonal mode expansion is evident when the output of the amplifier is dominated by the lowest order non-orthogonal mode. Then, the expression for the power, Eq.(3.10), can be approximated by

$$P \approx \Delta\nu\, \hbar\omega\, (B_{0,0}^{0})^2\, e^{2Re(\lambda_0^0)(\theta-\theta_0)} \tag{3.11}$$

From Eq.(3.11) we see that the gain of the dominant mode is determined from the real part of the eigenvalue λ_0^0. In the low gain regime the coupling between free space modes is very weak and thus the non-orthogonal modes are essentially the same as the free space modes. In this regime gain-guiding effects are not present so that in the region in which the lowest order mode is dominant the gain of the amplified field has precisely the same form as the scaled gain-length coefficient used in Chapter 2. However, as the gain of the amplifier is increased the coupling between free space modes becomes significant. In this regime there is an enhancement of the gain of the amplified field over the uncoupled gain result used previously. In Fig.13 we show a plot demonstrating the enhancement of gain in the dominant nonorthogonal mode; the vertical axis represents the gain of the dominant mode(normalized to gz) and the horizontal axis is the scaled gain-length parameter gz. The effect of gain enhancement for the dominant non-orthogonal mode is related to the mode coupling discussed by Perry *et.al.* and will be discussed in further detail in the next chapter.

In addition to gain enhancement, we find from Eq.(3.11) that the amount of noise effectively seeding the mode is greater than the usual quantum limit of 1 photon per mode by precisely the excess spontaneous emission or Petermann factor, $\left(B_{0,0}^{0}\right)^2$.

Though the dominant mode appears to have more than the usual one quantum of noise, it is not necessarily the case that the noise performance of the amplifier is affected. In fact Haus and Kawakami[32] have pointed out that if one injects a signal into the adjoint

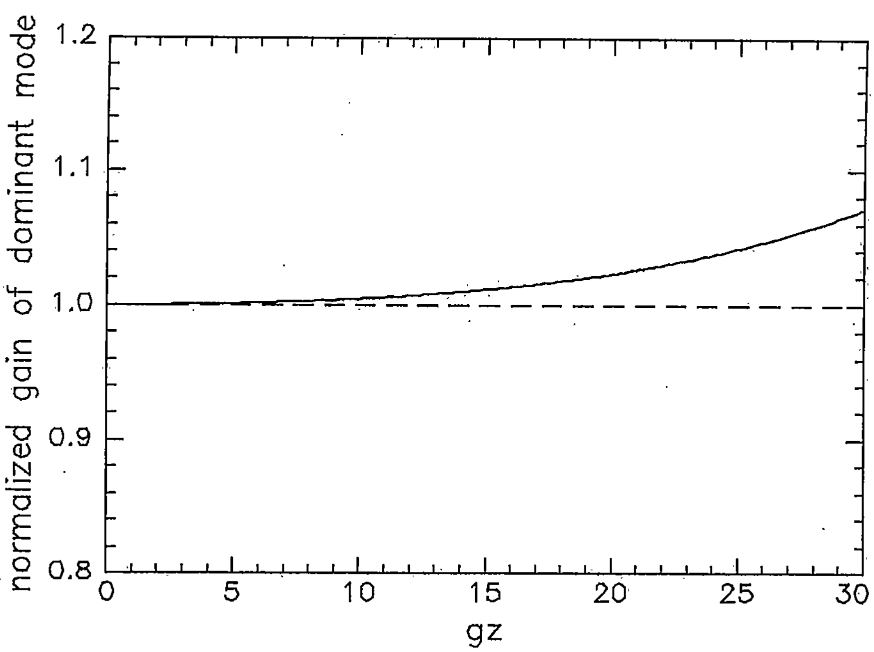

Figure 13 Normalized gain in dominant non-orthogonal mode vs. the scaled plane wave gain.

mode, ψ_0^0 , of the amplifier, the signal to noise ratio is not degraded by the Petermann factor.

In the following chapter we use this theory to analyze the results of two experiments in which the output of a Raman generator in a MPC were measured. The experiments, though similar in several respects to those presented in Chapter 2, are different in detail. The experiments were done at a much higher pressure so that we operated in regime of steady state SRS justifying the application of the nonorthogonal mode theory. In addition, to demonstrate the effects of gain-guiding we had to configure the experiments so that we could increase the gain, g, while leaving the scaled gain-length parameter essentially constant. This was done by decreasing the number of passes in the MPC.

CHAPTER 4

GAIN-GUIDING EFFECTS IN RAMAN AMPLIFICATION

The stimulated Raman process provides an excellent arena for studying the effects of gain-guiding on the noise properties of an amplifier. Though SRS has been actively studied since 1962[1] it is only recently that the effects of gain-guiding in SRS have been investigated both experimentally and theoretically. Using a single pass Raman amplifier Perry *et.al.* found that gain enhancement in the amplified Stokes field led to reduction of pump power needed to reach a given Stokes output.[18] Recently, Kuo *et.al.* used an non-orthogonal mode expansion of the Stokes field to describe the results of an experiment which examined beam pointing fluctuations in the output of a Raman amplifier.[37] They reported that excess noise in the Raman process influenced the beam pointing fluctuations.

In Chapter 2 we presented the results from several experiments in which the output energy of a Raman generator in a multipass cell was measured as a function of the pump input power. In that work it was found that for large gz the output could be reasonably described using a fully quantum mechanical plane wave theory of SRS, when the gain length coefficient, gz, was scaled to account for focusing and the multiple passes. However in the low gain regime where spontaneous Raman scattering was dominant, the simple plane wave theory failed because the total Stokes output contained a significant contribution from the spontaneous emission present in the higher order non-gaining spatial modes. Though the effects of gain-guiding were not manifest in this experiment, the results show that higher order spatial modes are coupled to the pump field which, as pointed out by LaSala *et.al.*,[38] is a necessary condition if gain-guiding effects are to be seen in higher gain regimes. Gain-guiding effects did not occur in that work because the pump intensities used were too small to get significant coupling between the higher order spatial modes.

In this chapter we report the results of an experiment that shows that gain-guiding effects can affect the noise properties of a Raman amplifier. To interpret our results we use the three dimensional theory of focused gain amplification derived in the previous chapter.

Experimental Results and Analysis

To demonstrate the effects of gain-guiding in an amplifier with focused gain we present the results from two experiments. In both experiments the output Stokes energy from a Raman generator in a multipass cell(MPC) was measured. A Raman generator is simply an amplifier with no input signal. Thus the output is due to amplified spontaneous emission only. The Raman generator, for these experiments, consisted of a cell of H_2 filled to 95 atmospheres pressure. The pressure was chosen so that the amplifier operated in the steady state regime since this is the regime in which the theory presented above is applicable. In steady state stimulated Raman scattering, the growth of the Stokes field is described using Eq.(3.2). The physical origin of the quantum Langevin term, $\hat{P}^{\dagger}_{sp}$, responsible for spontaneous emission, is the collision induced polarization fluctuations in the medium.[25]

The experimental apparatus used in both experiments was the same as used for the experiments presented in Chapter 2. However for completeness we present the diagram of the apparatus again(Fig.14). The essential details of the experiment are the same as those discussed in Chapter 2 and Appendix A. We did however replace the old YAG laser with an injection seeded Nd:YAG which provided increased stability as well as a larger dynamic energy range. The temporal profile of the new laser was near gaussian with a half width at half maximum (HWHM) of 2.5 ns. In Appendix E further details relevant to this experiment are given.

To compare the results of the experiment, in which the total energy of the Stokes pulse was measured, to the non-orthogonal mode theory, the instantaneous power given by Eq.(3.10), must be integrated over the temporal profile of the pump pulse. Additionally, to account for the spectral gain narrowing[25] in the Stokes pulse we use $\Delta\nu = \dfrac{\Gamma}{\pi\sqrt{gz}}$ for the full width at half maximum(FWHM) Stokes bandwidth in the

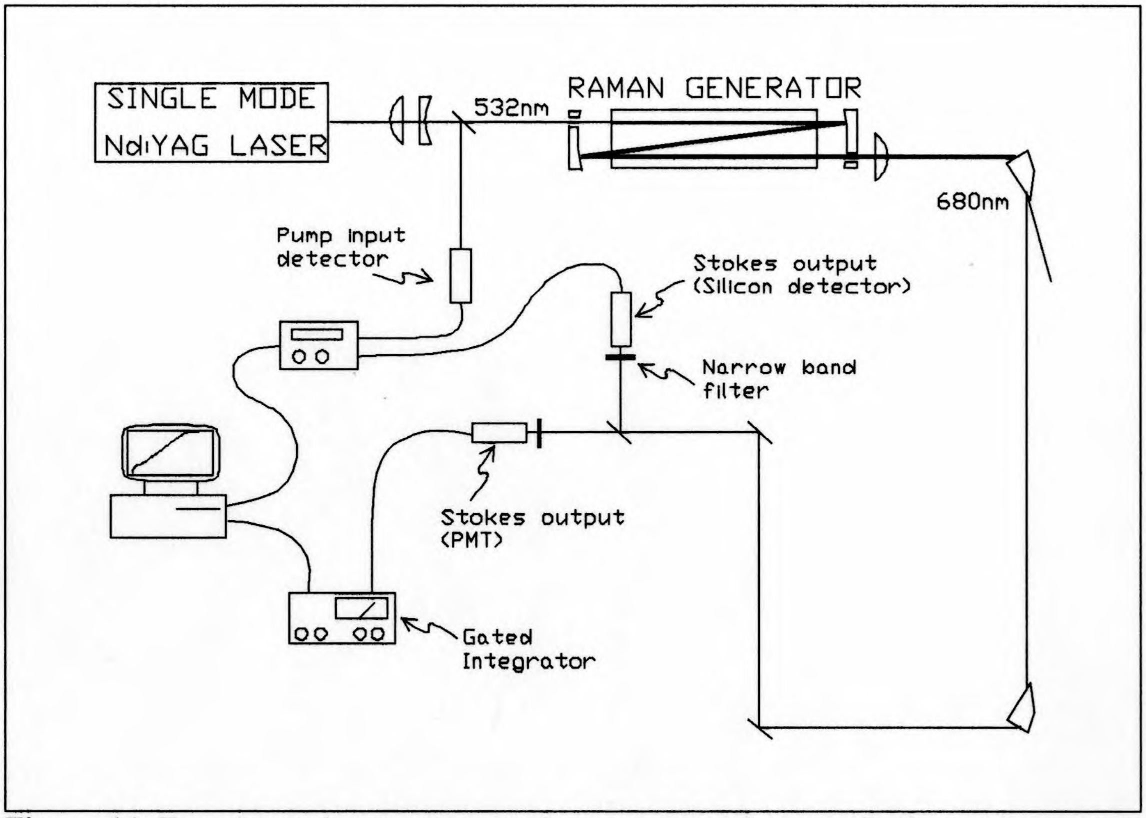

Figure 14 Experimental apparatus used to measure the growth from spontaneous emission in a Raman multipass cell.

calculation[16]; Γ is HWHM of the Raman linewidth and gz is the scaled gain length coefficient used in the previous calculations of Stokes amplification in a multipass cell.

Though the theory presented in the previous section was for a single focus geometry the results can be extended to account for multiple passes. In particular for the case in which each pass has the same confocal parameter, as was the case in these experiments, it is shown in Appendix D that the multiple passes can be accounted for by increasing the propagation parameter θ by the number of passes. We point out however that extending the results to multiple passes in this manner is strictly correct only for the case in which the mirrors are in the medium and there is no loss between passes. Thus even though we find excellent agreement between theory and experiment further studies need to be done to clarify the validity of this approach. To account for the loss between passes we used an effective number of passes given by Eq.(2.6). In addition, to discern when the effects of gain-guiding are important we also compare the results of our experiments to the fully quantum mechanical planewave theory of stimulated Raman scattering presented in Chapter 2.

As mentioned above in our first study of Raman amplification in a MPC gain-guiding effects did not play a role. The results from these experiments were successfully described using a plane wave theory of stimulated Raman scattering. The multiple passes were accounted for by extending the gain length product, gz, by the number of passes, while the effect of focusing was accounted for by scaling the plane wave gain coefficient. The scaling law was calculated based on the assumption that the Stokes pulse grows in only the lowest order gaussian mode and has the same confocal parameter as the pump.[23,24] Consequently the scaled gain coefficient used in those investigations was the same as the uncoupled gain coefficient discussed at the end of Chapter 3.

In Fig.15 the results of the experiment using the long cell (l_{cell}=141.5cm) are presented. The horizontal axis is the gain length product, gz, while the vertical axis is the output energy of the generator. The solid line is the output of the generator predicted by the non-orthogonal mode theory. As can be seen, the non-orthogonal mode theory fits the shape of the data quite well. Also plotted in Fig.15 as a dashed line is the plane wave theory, where, as mentioned earlier, the gain length coefficient has

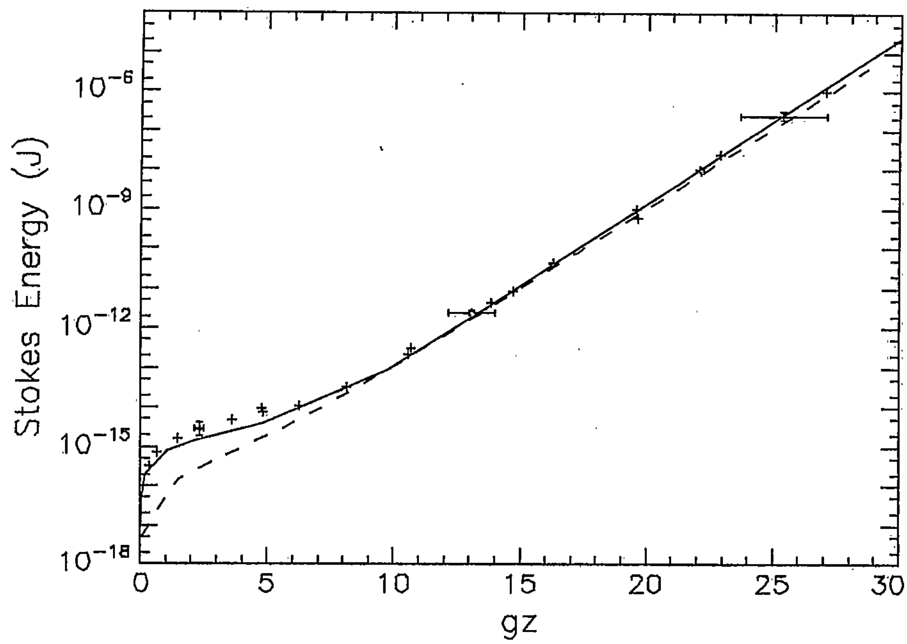

Figure 15 Stokes energy as function of the scaled gain-length parameter, gz. The experiment used a long Raman cell. The solid line represents the no-orthogonal mode theory while the dashed line represents the scaled plane wave theory.

been scaled to account for focusing and the multiple passes. For gz < 10 there is a substantial deviation from the scaled plane wave theory which is similar to what we found in Chapter 2. The increase in the Stokes energy is due to spontaneous emission in the higher order spatial modes, which are not accounted for in the plane wave theory. Because the gain in the higher order modes is less than the loss due to diffraction only the lowest order gaussian mode experiences exponential growth. In this experiment the coupling between the free space modes is negligible which implies that the lowest order non-orthogonal mode is approximately $\Phi_0^0(z,\boldsymbol{r}_T)\approx U_0^0(z,\boldsymbol{r}_T)$ over the whole gain range.

Consequently, for gz > 10, the Stokes output can be described by both the scaled plane wave theory(dashed line) and the non-orthogonal mode theory(solid line).

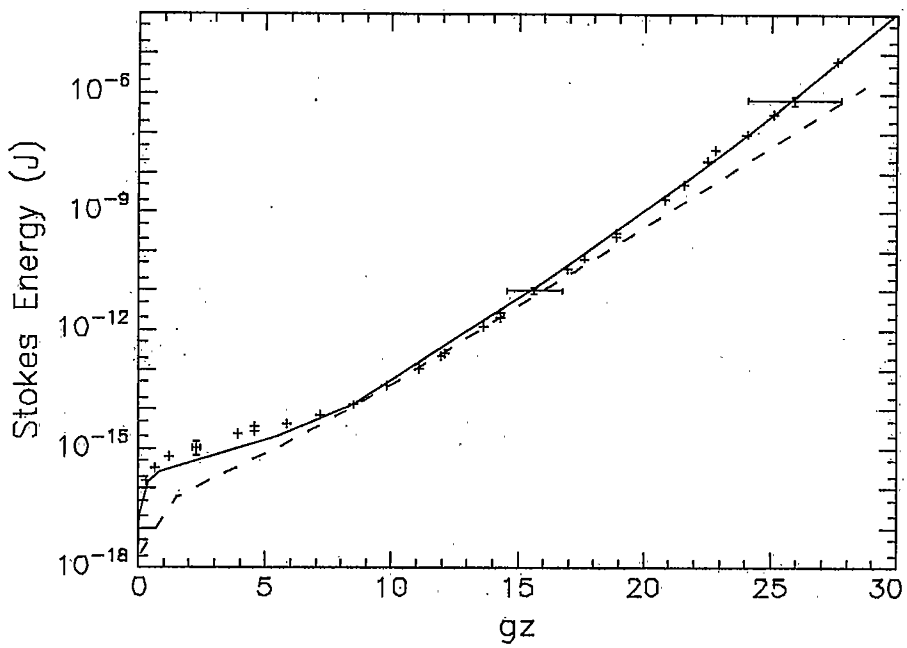

Figure 16 Stokes Energy as function of the scaled gain-length parameter, gz. The experiment used a short Raman cell. The solid line represents the non-orthogonal mode theory while the dashed line represents the scaled plane wave theory.

In Fig.16 the results of the experiment which used a short cell(l_{cell} = 25.4cm) are presented. Again we find a substantial deviation from the plane wave theory(dashed line) at low gz and as gz increases the Stokes growth initially follows the scaled plane wave theory. However, in contrast to the results of the long cell experiment, for gz ≥ 15 the Stokes gain becomes larger than the scaled plane wave gain. In this experiment the effect of gain-guiding is apparent; the Stokes growth is not described by the scaled plane wave theory, but is described by the non-orthogonal mode theory.

In the short cell experiment almost twice as much pump energy was needed to reach a given value of the gain length product, gz, than was needed for the long cell. The gain enhancement, first predicted by Perry *et.al.*,[22] occurs when the Raman cell is pumped hard enough that the gain in the higher order free space modes overcomes the loss due to diffraction. When the growth of the higher order free space modes is significant the Stokes field narrows in the transverse direction. This effect, referred to as transverse gain narrowing, is analogous to temporal mode locking in lasers.[41] Recall that in temporal mode locking the temporal modes of a laser act together to form a pulse which is narrower in time than the pulse would be if only one mode of the laser is used. By analogy transverse gain narrowing results when the transverse free space modes act together to form a new mode with a transverse profile which is narrower than the transverse profile of any one free space mode. This coherent superposition of free space modes is what results in the formation of the dominant non-orthogonal mode.

In the region where transverse gain narrowing occurs there is a significant coupling between the free space modes which implies that the dominant non-orthogonal mode, $\Phi_0^0(z,\boldsymbol{r}_T)$ can no longer be approximated by the lowest order gaussian free space mode. The amount of transverse narrowing expected in the short cell experiment is shown in Fig.17. The solid line is the transverse profile of the dominant non-orthogonal mode at the center of the Raman cell. For comparison, the transverse profile of the lowest order free space mode is also plotted (dashed line). The non-orthogonal mode pictured in Fig.15 has approximately 10% higher gain than the free space mode.

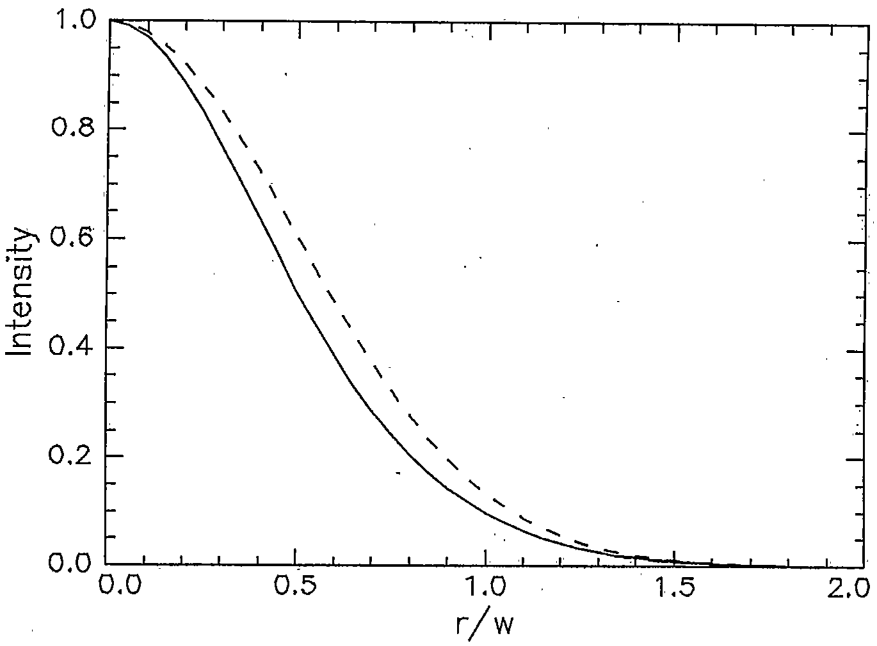

Figure 17 Comparison of the transverse spatial profile of the dominant non-orthogonal mode(solid line) to the transverse profile of the lowest order free space mode(dashed line).

In order to get a good fit to the data the theoretical plots in Fig.15 (Fig.16) were shifted up by a factor of approximately 5 (2). At this point it is not known if the needed offsets are an experimental artifact or some subtlety which has not been properly accounted for in the theory. However, it is clear from Fig.16 that gain guiding can affect the output of a Raman amplifier.

From the solution to the mode equation we are able to determine the Petermann factor for the dominant lowest order non-orthogonal mode. For this calculation we have assumed that the modes of the amplifier are defined by the peak pump intensity. In Fig.18 the Petermann factor is plotted as a function of the scaled gain length coefficient

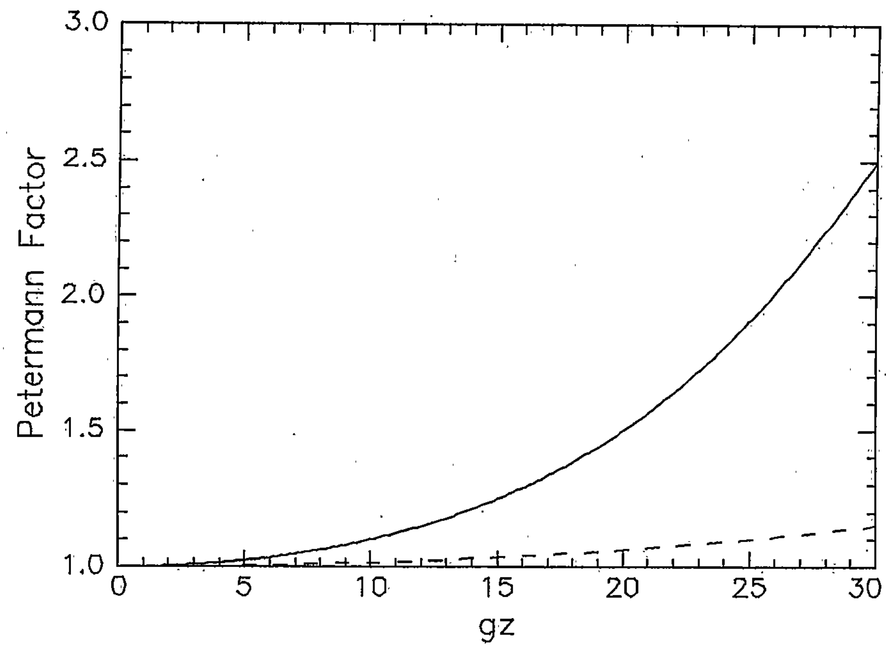

Figure 18 Petermann factor for both the short cell(solid line) and the long cell(dashed line) as function of gz.

for both the short cell (solid line) and the long cell (dashed line). The plot shows that the system begins with the usual one photon of noise per mode but, as gz increases, the coupling between the free space modes leads to an increase in the amount of spontaneous emission that effectively seeds the dominant non-orthogonal mode. The Petermann factor is much larger in the short cell experiment because, as discussed earlier, at high gain there is a significant increase in the population in the higher order free space modes contained in the dominant non-orthogonal mode.

The experiments presented do not directly probe the size of the excess noise factor or Petermann factor. However, calculation of the excess spontaneous emission factor in the region of enhanced gain show that effects associated with a Petermann factor as high as 2.5 should be present in the short cell experiment.

CHAPTER 5

SUMMARY

In Chapter 2 we were concerned with testing the limits of validity of the plane wave theory of Raman scattering. Our studies of the build-up of the Stokes intensity from quantum noise in a MPC indicate that the fully quantum mechanical transient plane wave theory adequately describes the SRS process for $gz \geq 10$. The scaling laws used to account for the focusing and multiple passes were the same used in previous experiments concerned with the amplification of a Stokes pulse in a MPC. We emphasize that in calculating the theory no free parameters were used; the plane wave gain coefficient and Raman linewidth, for the various pressures, were taken directly from empirical formulas given by Bischel and Dyer.[28,29] Though the predicted absolute intensity appears a little low for both pressures, the gain(slope) agrees remarkably well with experiment.

At lower gains we found a substantial deviation from the plane wave theory which we argue is due to the presence of higher order non-gaining spatial modes. To support this conclusion we present the results from a three dimensional theory by Perry *et al.*[22] which takes into account the effect of focusing and the multiple passes. The model is based on the solution to the steady state classical wave equation and therefore does not include the effect of temporal gain narrowing nor quantum initiation, inherent in the transient plane wave theory of Raymer and Mostowski.

In Chapter Three we developed a general three dimensional quantum theory of amplification for a focused gain geometry. The initial motivation for developing this theory was to explain, in a rigorous manner, the anomalous Stokes output measured in the low gain regime. In addition to accomplishing this the theory which is based on a non-orthogonal mode expansion of the amplified field also predicts that there can be excess noise in the output of a focused gain amplifier. We found that the excess noise takes the form of both enhanced gain and excess spontaneous emission in the output of the amplifier. Our analysis shows that as the gain in the non-orthogonal mode becomes larger than the scaled plane wave gain the amount of noise effectively seeding the mode is greater than the usual quantum limit of one photon per mode.

In Chapter Four we presented the results from two experiments which were designed to study the effects of gain-guiding on the noise properties of SRS. In those experiments we found that the gain of the output field was greater than the usual plane wave gain when the amplifier was pumped with large enough intensities such that significant coupling between the higher order spatial modes occurred. Though the results of these experiments do show the existence of enhanced gain they do not directly probe the size of the excess spontaneous emission factor.

Future

This thesis by no means constitutes a complete understanding of gain-guiding and its effect on the noise properties of a focused gain amplifier. In fact though we have answered many questions through this research we have, as is perhaps inevitable, found ourselves asking several more. In the next couple of paragraphs I point out several directions that are available for both theoretical and experimental investigation. The particular suggestions made are ones that I feel will further contribute to our understanding of quantum noise and fluctuations in gain-guided amplification.

On the theoretical front, as mentioned in Chapter 4, further consideration should be given to how the results of the theory should be extended to account for multiple passes. In particular, what are the effects of propagation outside the cell and the loss between cell windows? From my point of view a far more interesting avenue to pursue is how does the gain-guided or non-Hermitian character of the amplifier affect the noise performance of the amplifier. Specifically one can ask(and answer) how is the signal to noise(S/N) in the amplifier affected by the spatial structure of the injected signal? For example it has been shown that the S/N= $1/(B_{0,0})^2$ if a single photon is injected into the lowest order non-orthogonal mode. From this we conclude that the noise performance of the amplifier is degraded by the presence of excess spontaneous emission. However it has also been shown that if the photon is injected into the lowest order adjoint mode, referred to as adjoint mode coupling, that the noise performance is not degraded by the excess spontaneous emission factor, that is S/N = 1. What has not been explored, however, is how the S/N behaves if one injects a photon into the lowest order gaussian mode. Our preliminary calculations suggest that the S/N for the amplifier would be better than non-orthogonal mode coupling but not as good as adjoint mode coupling. Finally the combined effects of index and gain guiding should be explored rigorously. Again our preliminary work suggests that the effects of the index term, which can be realized experimentally, may have a significant effect on both the gain enhancement and the size of the Petermann factor.

With the advent of relatively cheap, stable, narrow linewidth, tunable diode lasers a wide variety of experiments have become accessible or at least more appealing. I think experiments concerned with determining the nature of the overall offset should be performed. In particular one should explore how varying parameters like the number of passes, cell length and cell pressure affect this offset. In each case a direct measurement of the offset could be made by noting at what injected intensities the output of the amplifier doubles the output when no signal is injected or, more concisely, at what injected intensities is the S/N = 1 for the amplifier. Once this effect is characterized experiments could be done testing the dependence of the amplifier S/N on the spatial structure of the injected signal. What is appealing about this experiment is that though much theoretical discussion has gone on about different coupling schemes there have been, to my knowledge, no direct measurements of the Petermann factor. Finally the effects of index guiding can be easily explored by tuning the injected signal over the Raman linewidth. As the signal is detuned the susceptibility picks up a real part which can be related to the index. By tuning to one side of resonance or the other the index can go from negative to positive, thus allowing the consequence of self focusing or focusing to be explored.

REFERENCES CITED

REFERENCES CITED

[1]N. Bloembergen, Amer. Journal of Physics **35**, 989, (1967).

[2]J. L. Carlsten and R. G. Wenzel, IEEE J. Quantum Electron. **19**, 1407, (1983).

[3]R. L. Byer and W. R. Trunta, Opt. Lett. **144**, (1978).

[4]P. Rabinowitz, A. Stein, R. Brickman, and A. Kaldor, Opt. Lett. **3**, 147, (1978).

[5]P. Rabinowitz, A. Stein, R. Brickman, and A. Kaldor, Appl. Phys. Lett. **35**, (1979).

[6]R. Sussman, Th. Weber, E. Riedle, and H. J. Neusser, Opt. Comm. **88**, 408, (1992).

[7]F. Y. F. Chu and A.C. Scott, Phys. Rev. A **12**, 2060, (1975).

[8]J. C. Englund and C. M. Bowden, Phys. Rev. Lett. **57**, 2661, (1986).

[9]C. M. Bowden and J. C. Englund, Opt. Commun. **67**, 71, (1988).

[10]D. C. MacPherson, R. C. Swanson, and J. L. Carlsten, Phys. Rev. A **40**, 6745, (1989).

[11]R. C. Swanson, D. C. MacPherson, P. R. Battle, and J. L. Carlsten, Phys. Rev. A **45**, 450, (1992).

[12]D. C. MacPherson, R. C. Swanson, and J. L. Carlsten, Phys. Rev. Lett. 61, 66, (1988).

[13]M. G. Raymer, Z. Li, and I. A. Walmsley, Phys. Rev. Lett. 63, 1586, (1989).

[14]M. D. Duncan, R. Mahon, L. L. Tankersley, and J. Reintjes, J. Opt. Soc. Am. B 7, 1336, (1990).

[15]I. A. Walmsley and M. G. Raymer, Phys. Rev. Lett. **50**, 962, (1983).

[16]R. C. Swanson, P. R. Battle, and J. L. Carlsten, Phys. Rev. Lett. **67**, 38, (1991).

[17]P. R. Battle, R. C. Swanson, and J. L. Carlsten, Phys. Rev. A **44**, 1922, (1991).

[18]B. N. Perry, P. Rabinowitz, and D. S. Bomse, Opt. Lett. **10**, 146, (1985).

[19]However, in the case of SRS it has been demonstrated that when the confocal parameter gets too small the threshold for first Stokes will begin to increase, due to the parametric coupling to the anti-Stokes field.

[20]D. C. MacPherson, R. C. Swanson, and J. L. Carlsten, IEEE J. Quantum Electron. **25**, 1741, (1989).

[21]For a review of molecular spectrascopic notation see for example Hetzberg, <u>Spectra of Diatomic Molecules</u>, published by Van Nostrand Reinhold Co.,(1950).

[22]B. N. Perry, P. Rabinowitz, and M. Newstein, Phys. Rev. A **27**, 1989, (1983).

[23]G. D. Boyd, W. D. Johnston Jr., and I. P. Kaminow, IEEE J. Quantum Electron. **5**, 203, (1969).

[24]W. R. Trutna and R. L. Byer, Appl. Opt. **19**, 301, (1980).

[25]M. G. Raymer and J. Mostowski, Phys. Rev. A **24**, 1980, (1981).

[26]The usual form of the intensity at the output of a Raman generator is given by[25]

$$I_s(\tau) = \frac{\Gamma g z\, |\gamma(\tau)|^2}{2} \Big\langle\, e^{-2\Gamma\tau}\left(I_0^2(\sqrt{q(\tau,0)}) - I_1^2(\sqrt{q(\tau,0)})\right) + 2\Gamma \int_0^\tau d\tau' e^{-2\Gamma(\tau-\tau')}\left(I_0^2(\sqrt{q(\tau,\tau')}) - I_1^2(\sqrt{q(\tau,\tau')})\right) \Big\rangle$$

where

$q(\tau,\tau') = 2\Gamma gz \int_{\tau'}^{\tau} d\tau'' \, |\gamma(\tau'')|^2$. Equation 5 is found by integrating the above expression

by parts.

[27]W. D. Fountain and M. Bass, IEEE J. Quantum Electron. **18**, 432, (1982).

[28]W. K. Bischel and M. J. Dyer, JOSA B 3, 677, (1986).

[29]W. K. Bischel and M. J. Dyer, Phys. Rev. A **33**, 3113, (1986).

[30]In the case of a single mode, the steady state Stokes energy, is[24]

$\varepsilon_s = \hbar\omega_s(e^{gz}-1)$, with $\hbar\omega_s$ = 2.91 x 10^{-19} J the energy of a Stokes photon in this work.

[31]K. Petermann, IEEE J. Quantum Electron. **15**, 566, (1979)

[32]H. A. Haus, and S. Kawakami, IEEE J. Quantum Electron. **21**, 63, (1985)

[33]A. E. Siegman, Phys. Rev. A **39**, 1253, (1989)

[34]I. H. Deutsch, J. C. Garrison, and E. M. Wright, J. Opt. Soc. Am. B **8**, 1244, (1991)

[35]P. Amendt, R. A. London, and M. Stauss, Phys. Rev. A **44**, 7478, (1991)

[36]W. A. Hamel and J.P. Woerdman, Phys. Rev. Lett. **13**, 1506, (1990)

[37]S. J. Kuo, D. T. Smithey, and M. G. Raymer, Phys. Rev. Lett. **20**, 2605, (1991)

[38]J. E. LaSala, D.A.G. Deacon, and J.M.J. Madey, Phys. Rev. Lett. **18**, 2047, (1987)

[39]Completeness of the non-orthogonal modes for the case of a focused gaussian profile, to our knowledge, has not been demonstrated. However, it appears that the non-

orthogonal modes are complete enough to describe the growth of Stokes field from spontaneous emission.

[40]This expression for the bandwidth is only valid at high gains.[25] At low gains the lineshape is Lorentzian, however for simplicity we approximate the bandwidth as $\dfrac{\Gamma}{\pi\sqrt{gz+1}}$.

[41]M. Suzuki and H. Tashiro, J. Opt. Soc. Am. B 8, 1686, (1991)

APPENDICES

APPENDIX A

DETAILS OF GENERATOR EXPERIMENT

In this appendix the details of experiment discussed in Chapter 2 are presented. The pump laser is a single mode frequency doubled Nd:YAG (Molectron model MY-3Y/MY-SAM) based on a design by Fountain and Bass,[26] though several modifications have been made to simplify the alignment.[20] We have also made additional modifications to increase the stability of the single mode operation. In addition to thermally isolating the laser we have mounted both the main cavity and sub-cavity optics on piezoelectric translator stages (Burleigh PZAT Aligner/Translator). The piezo devices are driven by two high voltage Burleigh drivers which are linked so that they can be driven simultaneously or individually. By monitoring the output of the laser in a Fabry-Perot we can make real time adjustments to the laser cavities to ensure single mode operation. In this manner we are able to keep the laser from mode hopping for periods lasting up to several minutes.

The temporal profile of the frequency doubled pump beam is gaussian with FWHM of approximately 17ns. To improve the spatial quality of the pump beam the output of the laser is focused through a tungsten wire die. The resulting spatial profile is near gaussian and is easily mode matched to the multipass cell. A Glan-air prism is placed at the output of the laser to ensure that the pump beam is linearly polarized. An optic placed after the spatial filter is used to pick off approximately 10% of the pump beam from which the energy is recorded for each shot. The total energy available at 532nm to pump the Raman generator is about 2mJ.

The two lens system before the MPC was used to mode match the pump beam to the MPC. The MPC design is the same as used in previous investigations[20] with the following modifications: the mirror spacing is now 1.95m, thus the mode matching confocal parameter is[20] b = 29cm, and the number of passes is increased to 17. The transmission of the MPC with the generator is measured directly using the pump beam and is found to be approximately 60%.

A lens at the output of the MPC is used to collimate both the pump and Stokes beam. The remaining pump is separated from the Stokes by two modified Pelin-Broca prisms and is discarded. The second prism is separated from the first by approximately 3 meters and is used to ensure that any anomalously scattered pump radiation is removed from the Stokes path. The Stokes pulse is then split and sent into both a silicon detector and a photomultiplier tube (PMT). In front of each of these detectors is a narrowband interference filter centered at the Stokes wavelength. The narrow band filters have a peak transmission of approximately 50% at the Stokes wavelength and a transmission of 10^{-4} at the pump wavelength.

The PMT (Hamamatsu R928) has a quantum efficiency of about 5% at the Stokes wavelength and is able to measure Stokes pulses with as many as 10^4 photons(femtoJoules) down to pulses with only a few tens of photons on average. The output of the PMT is connected to a gated integrator (EG&G model 165) which converts the current pulse to a voltage. After each shot the voltage on the integrator is digitized by a data acquisition board (National Instruments AT-MIO-9) and stored by a personal computer. The integrator is then cleared and readied for the next shot. For Stokes energies on the order of .1pJ or more, the silicon detector (Laser Precision RJP 765) becomes effective. The energy of each shot is recorded by an energy meter (Laser

Precision RJ 7620) and sent to the computer over a GPIB interface. As the PMT nears saturation a neutral density filter is placed in the beam path so that its effective energy range overlaps with the silicon detector. In this way the PMT can be calibrated to the absolute energy scale of the silicon detector. With this detection scheme we are able to detect the Stokes output over 12 orders of magnitude. As mentioned earlier, the pump energy is also monitored; the pump detector is a pyroelectric(Laser Precision RJP-735) which connects to the same energy meter as the silicon detector.

The plane wave gain coefficient and Raman line width are calculated using the work of Bischel and Dyer[27]. For 26.4 atmos. $\alpha = 2.93 \times 10^{-9}$ cm/W and at 3.2 atmos. $\alpha = 1.75 \times 10^{-9}$ cm/W. The Raman linewidth is calculated[28] to be $\Gamma/2\pi = 6.32 \times 10^{8}$ sec^{-1} at 26.4 atmos and $\Gamma/2\pi = 1.29 \times 10^{8}$ sec^{-1} at 3.2 atmos . The loss in the MPC and the Raman cell windows lead to an effective number of passes of approximately 13.

APPENDIX B

CALCULATION OF THE MODES IN A GAIN-GUIDED AMPLIFIER

In this appendix we derive an expression for the non-othogonal modes defined by Eq.(3.5). In addition we enumerate some of the properties and relationships between the non-orthogonal modes and the adjoint modes.

To solve explicitly for the modes of the system, we have found it useful to expand the mode $\Phi_n^l(z,\boldsymbol{r}_T)$ in terms of the free space, Gauss-Laguerre modes, $U_n^l(z,\boldsymbol{r}_T)$

which satisfy the slowly varying steady state free space wave equation,

$$\left(\nabla_T^2 - 2ik\partial_z\right)U_n^l(z,\boldsymbol{r}_T) = 0 \tag{B1}$$

Since this equation is Hermitian the usual completeness and orthogonality conditions hold for the free space Gauss-Laguerre modes,

$$\int d^2r_T\, U_{n'}^{l'*} U_n^l = \delta_{nn'}\delta_{ll'} \; . \tag{B2}$$

An explicit form for the free space modes in cylindrical coordinates is[22]

$$U_n^l(z,\boldsymbol{r}_T) = \frac{1}{w(z)}\left(\frac{2n!}{\pi(l+n)!}\right)^{1/2}\left(\frac{\sqrt{2}\,r}{w(z)}\right)^l L_n^l\left(\frac{2r^2}{w^2(z)}\right)\exp\left(-\frac{r^2}{w^2(z)} - i\left[\pm l\phi + \frac{kr^2}{2R} - (2n+l+1)\tan^{-1}\left(\frac{z}{z_o}\right)\right]\right) \tag{B3}$$

where $R(z)=z_o(z/z_o+z_o/z)$, $L_n^l(x)$ is an associated Laguerre polynomial and $w(z)$ is defined in the text. The indices n and l are associated with the radial and rotational indices respectively.

In the case of a general gain profile the modes of the gain-guided amplifier, $\Phi_n^l(z,\mathbf{r}_T)$, will not necessarily have the same symmetry as the free space modes. However, in the case of an axially symmetric gain profile the non-orthogonal modes have definite angular parity, just as the free space modes have definite angular parity. Since the gaussian gain profile given in Eq.(3.3) is axially symmetric, the modes $\Phi_n^l(z,\mathbf{r}_T)$ can be written as a sum over the radial part of the free space modes only,

$$\Phi_n^l(z,\mathbf{r}_T)=\sum_p b_{n,p}^l(z)\,U_p^l(z,\mathbf{r}_T) \quad . \tag{B4}$$

The free space mode coefficients, $b_{n,p}^l(z)$, are in general complex.

Substituting the above mode expansion into Eq.(3.3) and using the orthogonality relation, Eq.(B2), leads to an equation of motion for the free space mode coefficients given by

$$\partial_z b^l_{n,p'} - \frac{1}{2}\sum_p \left(\int dr_T^2\, U^{l*}_{p'} g(z,r) U^l_p\right) b^l_{n,p} = -\frac{2\lambda^l_n}{k_g w_g^2(z)} b^l_{n,p'} \quad \text{(B5)}$$

If the confocal parameter of the free space modes is chosen to be the same as the gain function then the gain function introduced in Eq.(3.3) can be expressed simply in terms of the lowest order free space mode, $g(z,r)=g_0|U^0_0|^2$. Using this form of the gain profile the second term in Eq.(B5), which represents the coupling between the free space modes, can be worked out explicitly. The details of this calculation are presented in Ref.22; the result is

$$\int dr_T^2\, U^{l'*}_{p'} g(z,r) U^l_p = \delta_{l,l'} \frac{g_o \mu}{\pi w_g^2(z)} e^{-2i(p'-p)\tan^{-1}(z/z_o)} Q^l_{p',p}(\mu) \quad \text{(B6)}$$

where $\mu = \dfrac{k}{k+k_g}$, and is referred to as the mode filling factor. $Q^s_{p',p}(\mu)$ in Eq.(B6) is a polynomial in μ only; its functional form is

$$Q^l_{p',p}(\mu) = \mu^l \left(\frac{p'!\,p!}{(p'+l)!\,(p+l)!}\right)^{1/2} \sum_{m=0}^{p} \binom{p+l}{m} \binom{p'+l}{m+p'-p} \frac{(p-m+l)!}{(p-m)} \mu^{2(p-m)} (1-\mu)^{2m+p'-p} \quad \text{(B7)}$$

where $p' \geq p$, but $Q^{l}_{p',p}(\mu)$ is symmetric with respect to interchange of p and p'.

Equation B6 shows that, for the choice of an axially symmetric, focused gaussian gain profile, modes which start in a state with definite angular parity will stay that way, which justifies letting the non-orthogonal modes have the same angular parity as the free space Gauss-Laguerre modes.

As pointed out by Perry *et.al.*[18,22] the key step in solving for the evolution of mode coefficients in a focused gain geometry is the change of variables $\theta = \tan^{-1}(z/z_o)$.

Using this variable change in Eq.(B5) gives

$$\partial_\theta b^{l}_{n,p'} - \sum_{p} b^{l}_{n,p} e^{-2ip'\theta} K^{l}_{p',p}(\mu) e^{2ip\theta} = \lambda^{l}_{n} b^{l}_{n,p'} \tag{B8}$$

where $K^{l}_{p',p}(\mu) = \mu\left(\frac{g_o z_o}{\pi w_g^2(0)}\right) Q^{l}_{p',p}(\mu)$. If the set of free space mode coefficients for the mode $\Phi^{l}_{n}(z, r_T)$ is denoted as a vector, $b^{l}_{n} = \{b^{l}_{n,p}\}$, and if $K^{l}_{p',p}(\mu)$ is written as a matrix, $\underline{K}^{l}$, then Eq.(B9) can be transformed to the operator equation,

$$(\partial_\theta - e^{-i\underline{H}\theta}\underline{K}^l(\mu)e^{i\underline{H}\theta} - \lambda_n^l)\boldsymbol{b}_n^l = 0 \tag{B9}$$

where $H_{p',p} = 2p\delta_{p'p}$

The solution to a similar equation has been presented in detail by Perry *et.al.*[22]. Using the same technique we find

$$\boldsymbol{b}_n^l = e^{-i\underline{H}\theta}\chi_n^l \tag{B10}$$

where the vector χ_n^l is a solution to the eigenvector equation given by

$$(\underline{K}^l + i\underline{H})\chi_n^l = \lambda_n^l \chi_n^l \tag{B11}$$

Using this solution the modes of system with gain may be calculated explicitly; in component form we find

$$\Phi_n^l(z,\boldsymbol{r}_T) = \sum_p e^{-2ip\theta} U_p^l \chi_{n,p}^l \ . \tag{B12}$$

<u>Some Properties of the Non-orthogonal Modes</u>

As shown above the eigenvectors, χ_n^l, of the operator $\underline{K}^l + i\underline{H}$ determine the spatial modes of the amplifier. The set of eigenmodes associated with the adjoint modes of the amplifier are found from the Hermitian adjoint of the operator $\underline{K}^l$+i$\underline{H}$,

$$(\underline{K}-i\underline{H})\gamma_n^l = \lambda_n^{l*}\gamma_n^l \quad . \tag{B13}$$

Some general properties of the eigenvectors follow from Eq.(B13) and its adjoint and are listed below,

$$B_{n,m}^{\;l} = \chi_m^{l*}\cdot\chi_n^l \tag{B14}$$

$$\gamma_m^{l*}\cdot\chi_n^l = \delta_{m,n} \tag{B15}$$

$$\gamma_n^{l*}\cdot\underline{K}^{\,l}\cdot\gamma_m^l = \frac{\lambda_m^{l*}+\lambda_n^l}{2}\gamma_n^{l*}\cdot\gamma_m^l \tag{B16}$$

where the dot implies the usual matrix multiplication. Using the fact that the free space modes are orthogonal and the bi-orthogonality property of the eigenmodes one can construct the adjoint mode to $\Phi_n^l(z,r_T)$. In component form it is given by

$$\psi_n^l(z,r_T) = \sum_p e^{-2ip\theta}\, U_p^{\,l}\gamma_{np}^l \quad . \tag{B16}$$

Thus the non-orthogonal modes and their adjoints obey the bi-orthogonality condition,

$$\int d^2r_T \Psi_n^{l*} \Phi_m^l = \delta_{n,m} \quad . \tag{B17}$$

Finally, because the operator, $\underline{\mathbf{K}}^l$+i$\underline{\mathbf{H}}$, is symmetric the eigenvectors are simply related to the adjoint modes by complex conjugation. For our particular choice of normalization we find that, $\gamma_n^{l*} = \chi_n^l$. The overlaps between the modes are therefore related by

$$\int d^2r_T \Phi_m^{l*} \Phi_n^l = \int d^2r_T \psi_n^{l*} \psi_m^l = B_{n,m}^l \quad . \tag{B18}$$

<u>**Structure of the non-orthogonal modes**</u>

In the limit of zero gain the non-orthogonal modes are simply related to the free space modes. However as the gain increases the non-orthogonal modes evolve into a coherent superposition of the free space modes. A natural question to ask is what do these modes look like. In Fig.(19) we compare the lowest order non-orthogonal mode width and radius of curvature(dashed line) to those of the lowest order free space modes(solid line). Note that the parameters were chosen to exaggerate the differences between the two modes. One difference between the two modes is that the non-orthogonal modes are narrower than the free space modes. This feature, called gain narrowing, results because the gain at the center of the gain profile is greater then in the wings of the gain profile. This phenomena is analogous to temporal mode locking in lasers. Recall that it is the coherent superposition of temporal modes in a laser which leads to a pulse which is narrower in time than any of the constituent modes. From Eq.(B12) we see that the non-orthogonal mode are simply a coherent superposition of free space modes; thus it is possible that they are narrower in space than the free space modes.

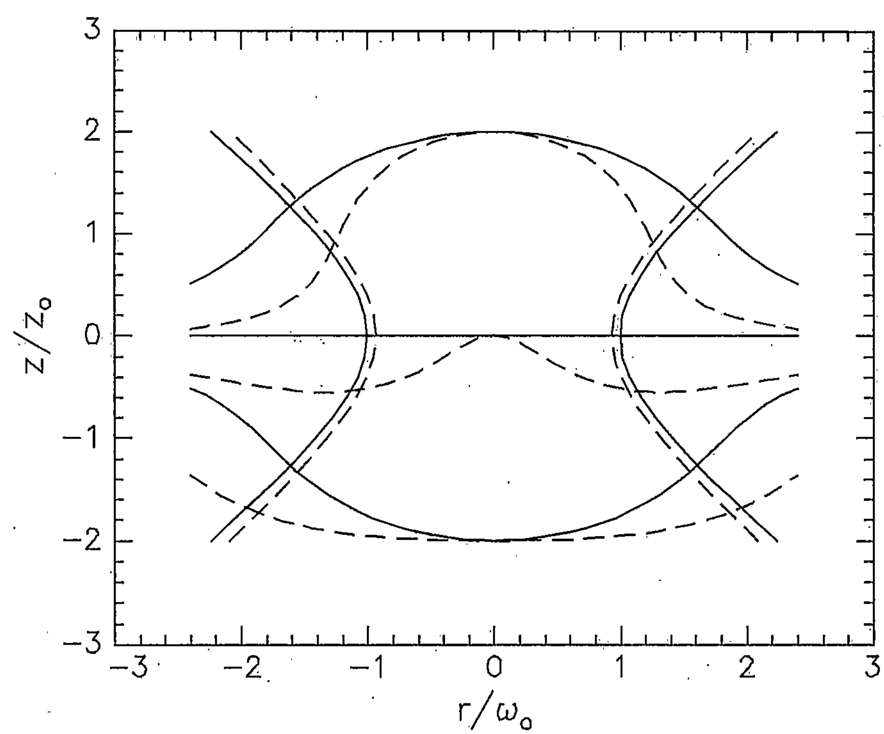

Figure 19 Comparison of beam width and radius of curvature between the lowest free space mode(solid line) and the lowest order non-orthogonal mode(dashed line). The direction of propagation is up.

The second more striking feature seen in Fig.19 is the difference in radius of curvature between the two modes. To understand why the non-orthogonal mode has this complex phase structure first consider a non-focused amplifier geometry. As the mode narrows, due to gain narrowing discussed above, it diffracts and thus generates a positive radius of curvature relative to the direction it is propagating. This is analogous to light passing through a narrow slit. Now add in the focused nature of the amplifier. Before focus the total radius of curvature can be thought of as the superposition of two components; a negative radius of curvature component which is associated with focusing and the positive component associated with gain-guiding. The net result is that the radius of curvature before focus is flatter than the gaussian mode. On the other side of focus the net radius of curvature is greater than the gaussian because the focused and gain guiding components are both positive .

APPENDIX C

SOLUTION TO THE MODE CORRELATION FUNCTION

In this appendix we derive an expression for the correlation function $<\hat{a}_n^{l\dagger}\hat{a}_m^{l}>$.

The result of this calculation can then be used in Eq.(3.9) to find an explicit expression for the power from a focused gain amplifier.

We begin by solving for the evolution of the operators, $\hat{a}_n^{l\dagger}$. To do this first multiply both sides of Eq.(3.8) by the adjoint mode ψ_n^{l*} and then integrate over the transverse coordinates. Using the bi-orthogonality of the modes, Eq.(B18), Eq.(3.8) becomes

$$\partial_\theta\left(e^{-\lambda_n^l\theta}\hat{a}_n^{l\dagger}\right)=\frac{2\pi k}{i}e^{-\lambda_n^l\theta}\hat{P}_{sp_n}^{l\dagger} \tag{C1}$$

where $\hat{P}_{sp_n}^{l\dagger}=\dfrac{k_g w^2(z)}{2}\int d^2r_T\psi_n^{l*}\hat{P}_{sp}^{\dagger}$. Formally solving Eq.(C1) and forming the correlation function for the mode operators yields,

$$<\hat{a}_n^{l\dagger}(\theta)\hat{a}_m^{l}(\theta)>=(2\pi k)^2e^{(\lambda_n^l+\lambda_m^{l*})\theta}\left[\int\!\!\int d\theta_1 d\theta_2 e^{-(\lambda_n^l\theta_1+\lambda_m^{l*}\theta_2)}<\hat{P}_{sp_n}^{l\dagger}\hat{P}_{sp_m}^{l}>\right]+e^{(\lambda_n^l+\lambda_m^{l*})(\theta-\theta_o)}<\hat{a}_n^{l\dagger}(\theta_o)\hat{a}_m^{l}(\theta_o)>$$

(C2)

The correlation function has a contribution from two terms. The first represents the correlation in the amplified spontaneous emission. The second term is the amplified correlation from the injected signal. In deriving Eq.(C2) we have implicitly assumed that the input field and amplified spontaneous emission are not correlated. Thus terms of the form $<\hat{P}_{sp}\hat{a}_n^{\dagger l}>$ are identically zero.

To proceed further an explicit expression for the correlation function $<\hat{P}^{l\dagger}_{sp_n}\hat{P}^{l}_{sp_m}>$ is needed. Its functional form depends on the particular mechanism used for amplifying the field. In this work the gain medium is modeled as an inverted two level amplifier. The model, though restrictive, has been used to describe a wide class of amplifiers, from the Raman amplifier[37] to a single pass X-ray laser[35]. For an inverted two level amplifier the steady state spontaneous polarization correlation function is[33,34]

$$\langle\hat{P}^{\dagger}_{sp}(z,\boldsymbol{r}_T)\hat{P}_{sp}(z',\boldsymbol{r}'_T)\rangle = \frac{\rho\hbar\Delta\nu}{2\pi k}g(z,r)\,\delta(z-z')\,\delta(\boldsymbol{r}_T-\boldsymbol{r}'_T) \tag{C3}$$

where $\rho = N_2/(N_2-N_1)$ is the inversion density and $\Delta\nu$ is the Hertzian bandwidth of the amplified field.

Using Eq.(C3) to solve for the Langevin correlation function in Eq.(C2) we find

$$<\hat{P}^{l\dagger}_{sp_n}\hat{P}^{\,l}_{sp_m}>=g_o\frac{\Delta\nu\rho\hbar}{2\pi k}\frac{w^4(z')k_g^2}{4}\delta(z'-z'')\int d^2r_T|U_0^0|^2\psi_n^{l*}\psi_m^l\ . \tag{C4}$$

Substituting the definition for ψ_n^l, given in appendix B, and the result from Eq.(B6), the above expression for the Langevin correlation function can be rewritten as

$$<\hat{P}^{l\dagger}_{sp_n}\hat{P}^{\,l}_{sp_m}>=\frac{\Delta\nu\rho\hbar}{2\pi k}w^2(z)k_g\delta(z'-z'')\gamma_n^{l*}.\underline{K}^l.\gamma_m^l \tag{C5}$$

where the dot between the vectors and the matrix represents the usual matrix multiplication. Finally combining Eqs.(B16) and (C5) and substituting this back into Eq.(C2) yields

$$\begin{aligned}<\hat{a}_n^{l\dagger}\hat{a}_m^l>&=\frac{2\pi\rho\Delta\nu\hbar\omega}{c}(\lambda_n^l+\lambda_m^{l*})\gamma_n^{l*}.\gamma_m^l e^{(\lambda_n^l+\lambda_m^{l*})\theta}\int_{\theta_0}^{\theta}d\theta' e^{-(\lambda_n^l+\lambda_m^{l*})\theta}+e^{(\lambda_n^l+\lambda_m^{l*})(\theta-\theta_o)}<\hat{a}_n^{l\dagger}(\theta_o)\hat{a}_m^l(\theta_o)> \\ &=\frac{2\pi\rho\Delta\nu\hbar\omega}{c}B^{\,l}_{m,n}\left[e^{(\lambda_n^l+\lambda_m^{l*})(\theta-\theta_0)}-1\right]+e^{(\lambda_n^l+\lambda_m^{l*})(\theta-\theta_o)}<\hat{a}_n^{l\dagger}(\theta_o)\hat{a}_m^l(\theta_o)>\end{aligned} \tag{C6}$$

where $\theta = \tan^{-1}(z/z_o)$. If we omit the second term, which is associated with the input signal, then Eq.(C6) is precisely the form of the correlation used in deriving the expression for the output power Eq.(3.10).

APPENDIX D

EXTENSION TO A MULTIPASS CELL

The expression for output power given in Eq.(3.10) is for single pass. In this appendix we show how to extend the results of the theory to multiple passes. Results are derived for two passes and then generalized to s passes. In particular we consider the case in which the amplifier is symmetric and each pass has the same confocal parameter, as diagramed in Fig.20. Since the MPC is mode-matched, the modes, Φ_n^l , are the same for each pass, up to an overall phase shift, so that only the generalized creation operator, $\hat{a}_n^{l\dagger}$, must be modified to account for the multiple passes.

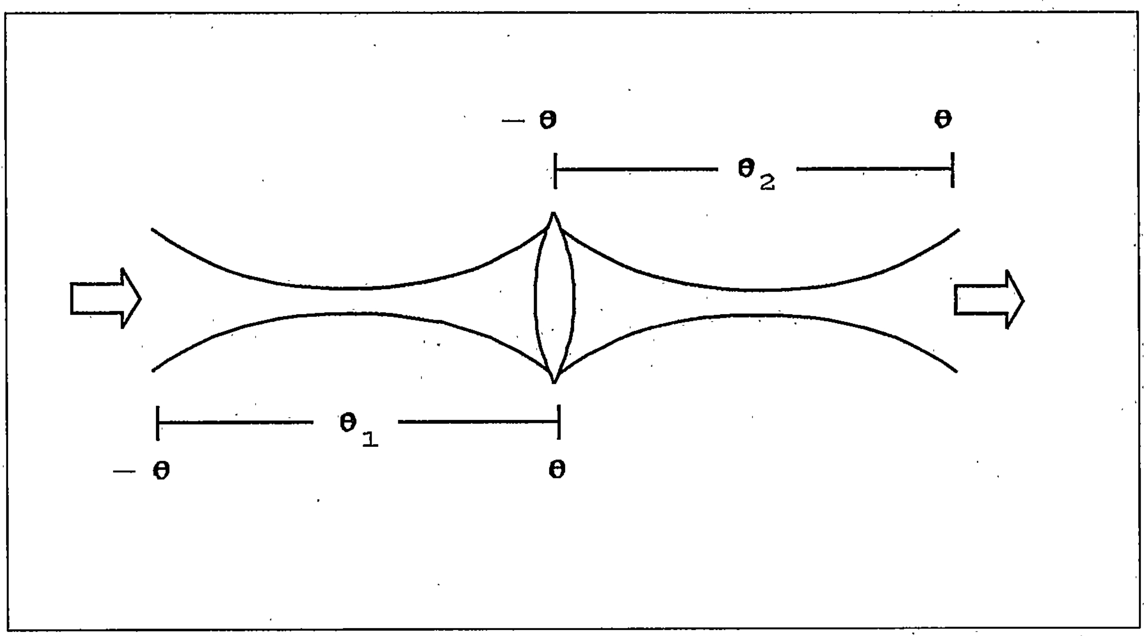

Figure 20 Diagram showing coordinates used in describing amplification in a multipass cell.

We begin by formally solving Eq.(C1) which gives an expression for the output of the first pass

$$\hat{a}_n^{l\dagger}(\theta_1=\theta) = \frac{2\pi k}{i} e^{\lambda_n^l \theta} \int_{\theta_1=-\theta}^{\theta} d\theta' \, e^{-\lambda_n^l \theta'} \hat{P}_{sp_n}^{l\dagger} + e^{2\lambda_n^l \theta} \hat{a}_n^{l\dagger}(\theta_1=-\theta) \quad . \tag{D1}$$

The first term on the right represents the spontaneous emission. The second term represents the amplified input, $\hat{a}_n^{l\dagger}(\theta_1=-\theta)$ being the value of the operator at the input to the amplifier. Equation D1 is general and thus can be used to obtain the output of any pass as long as the input to that pass is known. For two passes the generalized creation operator is

$$\hat{a}_n^{l\dagger}(\theta_2=\theta) = \frac{2\pi k}{i} e^{\lambda_n^l \theta} \int_{\theta_2=-\theta}^{\theta} d\theta' \, e^{-\lambda_n^l \theta'} \hat{P}_{sp_n}^{l\dagger} + e^{2\lambda_n^l \theta} \hat{a}_n^{l\dagger}(\theta_2=-\theta) \tag{D2}$$

where $\hat{a}_n^{l\dagger}(\theta_2=-\theta)$ is the input into the second pass. If we take the output of the first pass to be the input into the second pass then Eq.(D2) can be written as

$$\hat{a}_n^{l\dagger}(\theta_2=\theta) = \frac{2\pi k}{i} e^{\lambda_n^l \theta} \left[\int_{\theta_2=-\theta}^{\theta} d\theta' \, e^{-\lambda_n^l \theta'} \hat{P}_{sp_n}^{l\dagger} + e^{2\lambda_n^l \theta} \int_{\theta_1=-\theta}^{\theta} d\theta' \, e^{-\lambda_n^l \theta'} \hat{P}_{sp_n}^{l\dagger} \right] + e^{4\lambda_n^l \theta} \hat{a}_n^{l\dagger}(\theta_1=-\theta) \tag{D3}$$

From Eq.(D3) and its Hermitian adjoint we obtain the correlation function after two passes

$$
\begin{aligned}
<\hat{a}_n^{l\dagger}(\theta_2=\theta)\hat{a}_m^{l}(\theta_2=\theta)> &= (2\pi k)^2 e^{3(\lambda_n^l+\lambda_m^{l*})\theta} \int_{\theta_1=-\theta}^{\theta} d\theta''\, d\theta'\, e^{-(\lambda_n^l\theta'+\lambda_m^{l*}\theta'')} <\hat{P}_{sp_n}^{l\dagger}(\theta')\hat{P}_{sp_m}^{l}(\theta'')> \\
&+ (2\pi k)^2 e^{(\lambda_n^l+\lambda_m^{l*})\theta} \int_{\theta_2=-\theta}^{\theta} d\theta''\, d\theta'\, e^{-(\lambda_n^l\theta'+\lambda_m^{l*}\theta'')} <\hat{P}_{sp_n}^{l\dagger}(\theta')\hat{P}_{sp_m}^{l}(\theta'')> \\
&+ e^{4(\lambda_n^l+\lambda_m^{l*})\theta} <\hat{a}_n^{l\dagger}(\theta_1=-\theta)\hat{a}_m^{l}(\theta_1=-\theta)>
\end{aligned}
\tag{D4}
$$

In general, Eq.(D4) has nine terms. However, since the spontaneous emission from any pass is uncorrelated to the input and the spontaneous emission generated in different passes is statistically independent, six of the nine terms vanish. Each of the three terms in Eq.(D4) have clear physical interpretations: the first term represents the spontaneous emission generated in the first pass and amplified in the second pass, the second term is the spontaneous emission generated in the second pass, while the third represents the amplified input.

Eq.(D4) can be simplified further by assuming there is no input to the amplifier, thus the last term can be neglected. In addition if we make the usual change of variables z->θ in Eq.(C4) the spontaneous polarization correlation function can be expressed as

$$<\hat{P}^{l\dagger}_{sp_n}(\theta')\hat{P}^{\,l}_{sp_m}(\theta'')> = \frac{\rho\,\Delta\nu\,\hbar}{2\pi k}B_{m,n}(\lambda^l_n+\lambda^{l*}_m)\delta(\theta'-\theta'') \quad . \tag{D5}$$

Substituting Eq.(D5) into the two pass correlation function yields

$$<\hat{a}^{l\dagger}_m(\theta_2=\theta)\hat{a}^{\,l}_m(\theta_2=\theta)> = 2\pi k\rho\,\Delta\nu\,\hbar B_{m,n}\left(e^{4(\lambda^l_n+\lambda^{l*}_m)\theta}-1\right) \quad . \tag{D6}$$

For the case of s passes it is straightforward to show that the correlation function is simply

$$<\hat{a}^{l\dagger}_m(\theta_s=\theta)\hat{a}^{\,l}_m(\theta_s=\theta)> = 2\pi k\rho\,\Delta\nu\,\hbar B_{m,n}\left(e^{2s(\lambda^l_n+\lambda^{l*}_m)\theta}-1\right) \quad . \tag{D7}$$

Therefore we find that the multiple passes can be accounted for by simply scaling the propagation parameter θ by the number of passes.

APPENDIX E

DETAILS OF GAIN-GUIDING EXPERIMENT

In this appendix some of the details of the experiment presented in Chapter 4 are given. However because the experimental apparatus used in this work was simialr to that used for the experiments discussed in Chapter 2 the essential details have are ready been presented in appendix A and therefore are not repeated here.

The frequency doubled output of a pulsed, single mode Nd:YAG laser was used to pump the Raman generator. As mention earlier the laser in this experiment was an injection seeded Nd:YAG manufactured by Spectra-Physics. The temporal profile of this laser was approximately 2.5ns (HWHM). To improve the spatial quality of the pump beam, the output of the laser was focused through a tungsten wire die. The resulting spatial profile was gaussian which insured that the SRS gain profile would have the same gain profile(focused gaussian) as that used in the theory. In addition the the following modifications to the MPC set up were made; the mirror spacing was changed to 1.86m, the mode matching confocal parameter was $b = 2z_o$ =46cm, and the number of passes was reduced to 11. The transmission of the MPC including the Raman cell was measured directly using the pump beam and was found to be approximately 76% for the experiments presented in this chapter.

The plane wave gain coefficient, $\alpha = g/I_p$ and the Raman linewidth, Γ, are calculated from Bischel and Dyer[17]. At 95 atmospheres $\alpha = 2.944\text{x}10^{-9}$ cm/W and $\Gamma/2\pi = 2.12\text{x}10^{9}$ sec^{-1}. In both experiments the loss in the MPC and the Raman cell windows led to an effective number of passes of 9.6.

In both data sets presented, each experimental point represents approximately 100 shots all collected at a particular pump input energy (within ±2.5%). The transmission loss in the MPC as well as from the cell to the detectors were measured and folded out of the data, allowing a direct comparison with the theory. The error bars shown include both statistical and systematic errors and are representative of the size of the errors on all the points. The statistical errors are inherent in both the quantum nature of Stokes build up and in the fluctuations in detection caused by finite quantum efficiency of the detectors. The systematic errors arise from uncertainty in energy meter calibration and error in the measurement of transmission and reflection coefficients of the optical elements. For Stokes energies less than 10^{-14}J the vertical error bars are larger due to the uncertainty inherent in matching the output of the PMT to the absolute energy scale of the silicon detector.